University of Alberta

Library Release Form

Name of Author: Rahman Mohammadhassanpour

Title of Thesis: Tools for Multivariate Modeling of Permeability Tensors and Geometric Parameters for Unstructured Grids

Degree: Master of Science

Year this Degree Granted: 2007

_____

Rahman Mohammadhassanpour

Apt. 1006, 11025- 82 Ave.,
Edmonton, AB, T6G 0T1,
Canada

Date:_____

University of Alberta

Tools for Multivariate Modeling of Permeability Tensors and Geometric Parameters for Unstructured Grids

by

Rahman Mohammadhassanpour

A thesis submitted to the Faculty of Graduate Studies and Research
in partial fulfillment of the requirements for the degree of

Master of Science

in

Mining Engineering

Department of Civil and Environmental Engineering

Edmonton, Alberta

Fall 2007

University of Alberta

Faculty of Graduate Studies and Research

The undersigned certify that they have read, and recommend to the Faculty of Graduate Studies and Research for acceptance, a thesis entitled **Tools for Multivariate Modeling of Permeability Tensors and Geometric Parameters for Unstructured Grids** submitted by **Rahman Mohammadhassanpour** in partial fulfillment of the requirements for the degree of **Master of Science**.

_____
Dr. Oy Leuangthong

_____
Dr. Clayton V. Deutsch

_____
Dr. Carl Mendoza

Date:_____

Abstract

Geostatistical techniques produce fine scale models of facies and petrophysical properties to represent the geological heterogeneity and complexity. Direct use of large fine scale models in reservoir simulation is computationally expensive and inefficient. Generally, some coarsening or scale-up operations are required to generate suitable models for flow simulations. This process often requires unstructured grids and permeability tensors that are computationally complex to calculate for large 3D reservoir models.

Using multivariate statistics for direct simulation of permeability tensors for unstructured grids is a new research avenue. This requires calculating the permeability tensor and other geological and geometric parameters for unstructured grid blocks to build the required multivariate distribution.

The objective of this work is to build the required tools for multivariate modelling of permeability tensors and geologic and geometric parameters for unstructured grid blocks. This thesis proposes methods for: (1) accounting for geological heterogeneity within and between unstructured grid blocks, (2) calculating permeability tensors on unstructured grid elements, and (3) determining directions of geological continuity and unstructured grid geometry.

Acknowledgments

My deepest thanks go to my supervisor, Dr. Oy Leuangthong, for her precious guidance, encouragement and support. I also want to extend my sincere thanks to my advisor, Dr. Clayton V. Deutsch. Completion of this thesis wouldn't be possible without his insightful guidance and helps.

I appreciate the support of my colleagues at the Centre for Computational Geostatistics, especially my dear friend, Hadi Derakhshan, for his friendship, encouragement and long-time support.

I would like to thank my parents (Reza and Parvaneh) for their love, understanding and support. Finally, I dedicate this thesis to my wife, Shima, for her love, support and being the source of strength and inspiration throughout my study.

Table of Contents

List of Figures

Chapter 1 : Introduction

1.1 Problem Setting

The main objective in describing a reservoir is the characterization of heterogeneities that influence the flow of fluids through the reservoir. Geostatistical methods are used in order to integrate geological, geophysical, and petrophysical information to make inferences about static reservoir properties at unsampled locations. Generally, geostatistical realizations provide models of reservoir properties for millions of grid blocks to better capture heterogeneity based on multiscale information. These reservoir models can then be used in reservoir simulation for flow prediction. However, due to the limitation in flow simulators, using large fine scale models for flow simulation is impractical and inefficient. Thus, flow simulation grids are often selected coarser than the geostatistical modelling cells. Some coarsening or upscaling techniques must be applied in order to average the fine scale properties to coarse blocks (Prevost, 2003).

The coarse flow simulation grids can be either regular or unstructured. Unstructured grids are becoming more commonly used in flow simulation in order to resolve complex features such as faults, channels or reservoir boundaries. Using this kind of grids leads to more accurate flow simulation results (Verma and Aziz, 1997); however, characterization of properties such as permeability for unstructured grids is more time consuming and requires further considerations. This is due to the fact that irregularly shaped grids do not conform to the underlying fine scale model and this irregularity changes the assumption of simulators which consider that the pressure equation has a diagonal permeability tensor. Flow simulation on unstructured grids

requires directional permeability or full tensor permeability to be specified (Edwards, 1998).

Different approaches are often used to characterize reservoir properties on unstructured grid blocks. The most common approach is to first generate appropriate fine scale properties such as facies, porosity and permeability using geostatistical modelling. Then the fine scale model is subjected to flow simulation. The fine scale flow results and all geological and engineering information are gathered to generate the coarse unstructured grid model. The last step is to upscale the fine scale model to coarse grid blocks (Prevost, 2003). This procedure is computationally expensive and complex for large 3D reservoir modelling (Wen et al., 2003).

Direct simulation is another approach. The idea of direct simulation is to simulate in the original data unit in order to avoid transformation (to Gaussian unit) and to account for data of various support volume (Manchuk et al., 2004). Direct simulation of permeability tensor on an unstructured block scale requires the multivariate distribution of permeability tensor, geological parameters and geometric parameters of unstructured grids. Examples of geological parameters are geological facies proportion, average petrophysical properties and direction of continuity; an example of grid geometric parameters is the orientation of grid blocks according to the coordinate system and grid volume. Here the main idea is to calculate these parameters for some representative unstructured grid, build the multivariate distribution, and then use this distribution and Monte Carlo simulation to estimate for all unstructured blocks.

The focus of this work is on the first part which is related to the development of new tools for calculation of geological and geometric parameters. These tools can be used to create data points for informing the multivariate distribution by processing high resolution training images through flow simulation.

1.2 Grids in Flow Simulation

Solving the flow equations with numerical approaches requires discretizing the reservoir system into a set of grid blocks. Various types of grid specifications exist for the purpose of flow simulation. There are generally two common kinds of grid; regular grid and unstructured grid. This section briefly reviews the different types of flow simulation grids that one may be confronted with in the numerical modelling process.

1.2.1 Regular Grid

Regular Cartesian grids are used most commonly in reservoir simulation (Aziz, 1993). The grid blocks are generated along the orthogonal coordinate directions. The identifying point of a grid can be either located at the center of block (block-centered) or any other location inside the block (point-distributed). The block size can be different from one location to another location. Regular grids are usually preferred in flow simulation due to the simplicity. Figure 1.1 shows an example of regular grids.

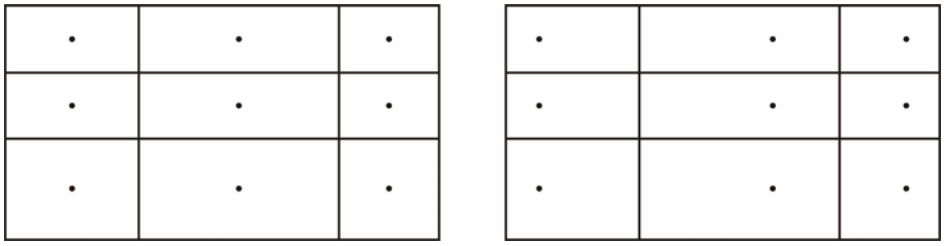

Figure 1.1 Regular Cartesian Grids. Block-centered (left) and point-distributed grids (right) (redrawn from Aziz, 1993).

1.2.2 Unstructured Grid

Reservoir geometries are usually not convenient enough to be discretized by a regular Cartesian grid. Unstructured grids are widely used in such complex reservoir geometry. Today's reservoir simulators are capable of handling irregular grids such as

corner point geometry, and PEBI (Perpendicular Bisection) or voronoi grids (Palagi and Aziz, 1991). An example of an unstructured grid is shown in Figure 1.2.

Corner point grids are the most popular unstructured grid and are often used in complex field studies. The grids basically have a polygonal shape and are specified with the coordinates of each vertex. The flexibility in shape provides a good adaptation to the reservoir boundary, faults or horizontal wells while preserving the simplicity of calculating the geometric quantities in flow equation (Aziz, 1993).

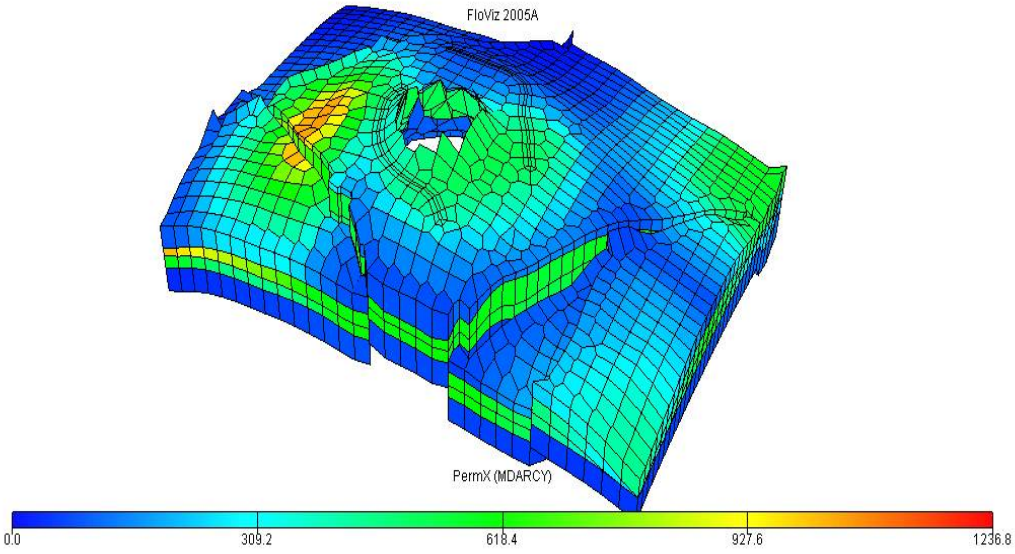

Figure 1.2 An Example of an Unstructured Grid Model (Source: Eclipse Floviz 2005A, Tutorial)

1.3 Tensors and Principal Directions

An anisotropic medium is one in which the value of a property is direction dependent. Tensors are commonly used to show the value of an anisotropic property with respect to all coordinate axes. They are widely used in mathematics and physics. In mechanics, tensors are used to describe the strain, stresses and the moment of inertia. In petroleum engineering, the directional rock permeability is characterized as a tensor.

Tensor is a 2 by 2 matrix in 2D or a 3 by 3 in 3D cases. The main diagonal component of each tensor indicates the value of anisotropic variable in the principal coordinate axes (e.g. *X*, *Y* and *Z* Cartesian coordinates) while the off-diagonal terms shows the value with respect to other arbitrary axes.

Given the components of the symmetric tensor in a coordinate system, we can find all components in any other coordinate system. Consider an anisotropic property, *A*, in an anisotropic medium. The value of variable *A* based on the coordinate axes of *X*, *Y* and *Z* is shown with the following symmetric tensor:

$$A = \begin{bmatrix} A_{xx} & A_{xy} & A_{xz} \\ A_{yx} & A_{yy} & A_{yz} \\ A_{zx} & A_{zy} & A_{zz} \end{bmatrix} \tag{1.1}$$

in which $A_{xy} = A_{yx}$, $A_{xz} = A_{zx}$ and $A_{yz} = A_{zy}$.

For a new coordinate system (*X*', *Y*' and *Z*') which is orientated at an angle θ apart from the original axes the relationship can be derived (Beer et. al., 1988). For the two dimensional case, these relationships are:

$$A_{x'x'} = \frac{A_{xx} + A_{yy}}{2} + \frac{A_{xx} - A_{yy}}{2}\cos 2\theta - A_{xy}\sin 2\theta \tag{1.2}$$

$$A_{y'y'} = \frac{A_{xx} + A_{yy}}{2} - \frac{A_{xx} - A_{yy}}{2}\cos 2\theta + A_{xy}\sin 2\theta \tag{1.3}$$

$$A_{x'y'} = \frac{A_{xx} - A_{yy}}{2}\sin 2\theta + A_{xy}\cos 2\theta \tag{1.4}$$

where $A_{x'x'}, A_{y'y'}$ and $A_{x'y'}$ are the component of tensor in new coordinate system.

Equation (1.2) and (1.4) are the parametric equation of a circle. This circle is called Mohr's circle. Figure 1.3 shows an example of Mohr's circle. Mohr's circle shows the variation of tensor components when the angle θ is changing. According to this circle we can find an angle θ such that the cross terms become zero and the tensor is diagonal ($A_{x'y'} = A_{y'x'} = 0$). Points B and D on the circle show two cases where the tensor is diagonal and $A_{x'x'}$ is minimum and maximum, respectively. Those directions that have these properties are called the *principal directions* of the tensor. The angle θ can be defined by the following formula:

$$\tan 2\theta = -\frac{2A_{xy}}{A_{xx} - A_{yy}} \tag{1.5}$$

The equation defines two values of 2θ which are 180° apart and thus two values of θ which are 90° apart. In order to define which angle is related to $A_{\max}$ and which one is related to the $A_{\min}$, we can substitute both values of θ into equation (1.2) and define the maximum value of *A*.

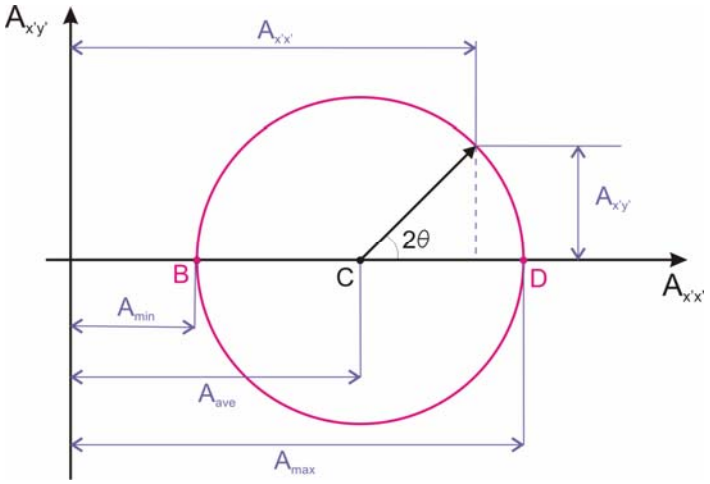

Figure 1.3 Mohr's Circle (redrawn from Beer et. al., 1988)

For three dimensional tensors, the principal directions can be defined by eigenvalue and eigenvector decomposition. This requires solving the following equation:

$$\begin{bmatrix} A_{xx}-\lambda & A_{xy} & A_{xz} \\ A_{yx} & A_{yy}-\lambda & A_{yz} \\ A_{zx} & A_{zy} & A_{zz}-\lambda \end{bmatrix} . \begin{bmatrix} v_x \\ v_y \\ v_z \end{bmatrix} = 0 \qquad (1.6)$$

where v_x, v_y and v_z are the components of the eigenvector in the principal direction and λ is the corresponding eigenvalue.

The three eigenvalues of equation (1.6) are the roots of the following cubic equation:

$$\begin{vmatrix} A_{xx}-\lambda & A_{xy} & A_{xz} \\ A_{yx} & A_{yy}-\lambda & A_{yz} \\ A_{zx} & A_{zy} & A_{zz}-\lambda \end{vmatrix} = \lambda^3 - a\lambda^2 + b\lambda - c = 0 \qquad (1.7)$$

where the coefficients are:

$$\begin{aligned} a &= A_{xx} + A_{yy} + A_{zz} \\ b &= A_{xx}.A_{yy} + A_{yy}.A_{zz} + A_{xx}.A_{zz} - A_{xy}^2 - A_{yz}^2 - A_{xz}^2 \\ c &= A_{xx}.A_{yy}.A_{zz} + 2A_{xy}.A_{yz}.A_{xz} - A_{xx}.A_{yz}^2 - A_{yy}.A_{xz}^2 - A_{zz}.A_{xy}^2 \end{aligned} \qquad (1.8)$$

Once the eigenvalues are calculated, the eigenvectors are determined by substituting them into equation (1.5). Finally we have three eigenvalues and three corresponding eigenvectors which represent the principal directions. It has been shown (Beer et. al., 1988) that the eigenvalues are the values of the variable *A* in the principal directions. Based on this, the major principal direction is related to the one with the greater eigenvalue.

1.4 Thesis Outline

The objective of this work is to generate the appropriate tools to calculate the required parameters for multivariate modelling of permeability tensor on unstructured grid

elements. These parameters are facies proportion, permeability tensor, geological continuity direction and unstructured block orientation.

In Chapter 2, different methods of geological facies modelling are reviewed and a methodology is proposed for accounting for geological heterogeneity within and between coarse unstructured grid blocks. A conventional indicator kriging and simulation approach is used to simulate connected blocks one at a time, with successively increased conditioning to previously simulated locations.
In Chapter 3 the available upscaling techniques are reviewed and a new flow-based upscaling method based on a numerical finite difference solution of the steady state flow equations, random boundary conditions and optimization is applied.

In Chapter 4 the methodology for determination of continuity direction in geological setting and also the unstructured grid element is presented. Moment of inertia concept is used to automatically determine the geological continuity direction and orientation of an unstructured grid element.

Chapter 5 summarizes the results and addresses other research ideas as a result of this work.

Chapter 2 : Geological Heterogeneity Modelling

Conventional reservoir modelling permits heterogeneity characterization of different aspects of the reservoir and involves several modelling tasks. It is common to begin by defining the key structural features, such as relevant horizons and fault block(s). Geological facies distributions between horizons and within fault blocks are then considered. Finally, petrophysical properties, such as porosity and permeability, are then characterized within these defined facies. This is a fairly standard procedure, and assumes that staitionarity of the petrophysical properties is valid within each facies. Geostatistics permits heterogeneity modelling within a stationary domain and since the facies model fundamentally defines these stationary zones, we can consider that the petrophysical distribution within a facies is heterogeneously homogeneous. As a result, the facies model which can be constructed via geostatistics captures a higher (macroscopic) level of heterogeneity (Caers, 2005).

In this chapter we review the available facies modelling techniques. A different approach is examined for facies modelling within the coarse regular and unstructured grid blocks followed by some sensitivity analyses.

2.1 Background

The reservoir architecture is represented by heterogeneity modelling techniques. Three main approaches are typical: cell-based modelling, object-based modelling and most recently, multiple point geostatistics using training images. Of the three primary approaches to facies modelling, cell based models remain the most common in practice.

2.1.1 Cell-based Facies Modelling

In cell-based modelling, the reservoir volume is commonly discretized into a regular Cartesian grid and relies on the two-point variogram statistic to capture structural correlations. Indicator and truncated Gaussian methods are common in this class of techniques; the former indicator approach is more common in practice. Indicators are widely used in modelling categorical variables because the distribution of uncertainty can be estimated directly (Journel, 1983). The categorical facies data are transformed into a binary variable via the following transform:

$$i(\mathbf{u}_\alpha; k) = \begin{cases} 1, & \text{if facies } k \text{ is present at } \mathbf{u}_\alpha \\ 0, & \text{otherwise} \end{cases}$$

where $k=1,\ldots,K$ categories, and $\mathbf{u}_\alpha$ represents a location in domain $\mathcal{A}$. The mean indicator and variance are then defined as:

$$E\{i(\mathbf{u};k)\} = p_k$$

$$Var\{i(\mathbf{u};k)\} = p_k(1-p_k)$$

where p_k is proportion of Facies k within the domain.

Inference using indicators can be performed in one of two modes: estimation and simulation. In the former case, indicator kriging (IK) yields the estimated probability of each threshold at unsampled locations:

$$p_k^*(\mathbf{u}) = \sum_{\alpha=1}^{n} \lambda_\alpha \left[i(\mathbf{u}_\alpha; k) - p_k \right] + p_k$$

where λ_α is the weight assigned to the indicator value at location $\mathbf{u}_\alpha$. In the latter case, sequential indicator simulation (SIS) permits global and local uncertainty to be assessed on the reservoir model (Seifert et. al., 1999). Note that the estimation with indicator results in a continuous attribute (a probability), while SIS results in realizations that consist of categorical values (that represent a specific facies).

Truncated Gaussian simulation is another cell-based facies model. Matheron et al. (1987) proposed this method. In this method, spatial distribution of categorical variables is modeled using a continuous multi-gaussian random function. Truncation is applied at a series of thresholds to create categorical facies realizations. The advantage of this simulation technique is that ordering relationships may be reproduced. However, the indicator variogram reproduction is not good because simulation is based on only one variogram.

Truncated pluri-gaussian simulation (Galli et al., 1994; Le Loc'h and Galli, 1997) is an extension of truncated Gaussian simulation which allows simulation of more complex geometry of lithofacies. More variables are simulated by considering multiple random functions and then the multivariate distribution is truncated.

2.1.2 Object-based Facies Modelling

Object-based models are suitable when geo-body geometries are well understood and can easily be specified using simple objects. It is primarily a boolean simulation wherein geo-objects are stochastically populated within the model; the presence of many conditioning wells can be problematic and remains a long-standing challenge to these approaches (Deutsch, 2002). The fluvial setting is a common example of reservoirs which are modeled with the object-based techniques (Omre, 1992; Georgsen and Omre, 1993; Hatloy, 1995). FLUVSIM is an object-based algorithm for building stochastic fluvial ribbon models (Deutsch and Wang, 1996; Deutsch and Tran, 2002). The method produces realistic models, but is inefficient at honoring a realistic level of conditioning data.

2.1.3 Multipoint Geostatistics

Multiple point geostatistics has received much attention recently and relies on extracting multiple point statistics derived from training images. This technique was first proposed by Journel and Alabert (1989) and then used in simulation by Deutsch

(1992). Single normal equation simulation (SNESIM) is an efficient multiple-point geostatistical algorithm which was firs proposed by Guardiano and Srivastava (1993) and then improved by Strebelle (2002).

The main idea is to select a template of *n*-points and then calculate the conditional probabilities of an outcome by scanning the template over the training image. The method does not require a variogram. The variogram and histogram are implicit to the training image. The method can yield a realistic geology model, but relies heavily on the training image thus representativity of the image is an important issue.

2.2 Proposed Methodology

Suppose that a large reservoir model is to be constructed using an unstructured grid. Using this kind of grid will almost certainly introduce different block sizes in the field of study. A fine grid is needed in parts of the reservoir where saturation and pressure changes rapidly, such as near wells and faults. However, there is no need to discretize the whole reservoir with a very fine grid and some parts can be discretized by coarser grids. This may help to reduce the computational storage, effort and time in flow simulation.

Geologic heterogeneity is generally not an issue for fine scale blocks since a sufficiently small block may be adequately characterized by a single facies. However, as the block scale becomes progressively larger as we move away from wells, these coarser blocks may consist of multiple facies and/or geologic sequences. A geologic description of these coarser blocks must inherently require statements regarding constituent facies proportions; this information, however, is insufficient to capture the facies continuity within and between these coarse blocks. This heterogeneity is important because they may have an impact in the hydrocarbon flow between wells and/or across faults. There is a need to capture the heterogeneity of irregularly-shaped

multiscale blocks, particularly if coarse scale blocks encompass multiple facies or even multiple sequences. As such, the following methodology is proposed:

1) Perform indicator kriging on the entire field conditioning to the facies data from wells. This yields the local facies proportion at each grid block, and forms the only information available for coarse grid blocks.
2) Refine the geological heterogeneity for a chosen coarse grid block via:
    a. Choose an appropriate fine scale resolution for this grid block.
    b. Perform sequential indicator simulation conditioned on the well data and the local facies proportions from Step (1) above for this refined grid.
    c. Add this locally refined grid simulation to the database and proceed to the next coarse block chosen for selective refinement. Refined simulation of all subsequent coarse blocks will be conditioned on (i) original well data, (ii) local facies proportion for that coarse block, and (iii) any nearby previously refined coarse blocks.

2.3 Application to Unstructured Block

Since the conventional geostatistical methods are based on a Cartesian grid, the proposed method cannot be directly applied to an unstructured grid. One straightforward idea is to approximate an unstructured block using a fine Cartesian grid, and then performing SIS for this fine scale grid. In this case each coarse unstructured block is locally refined by a high resolution point scale grid. An example will be presented in the next section.

2.4 Synthetic Examples

In order to check the validity of the methodology, two examples are considered. In the first example regular coarse blocks are considered. In the second example, connected unstructured blocks are examined.

2.4.1 Regular Blocks

Consider a field whose extents are 2000 *m* in Easting (X), 2000 *m* in Northing (Y) and 15*m* in the vertical (Z) resolution. Geological survey shows that there are three different sequences in this field: S1, S2 and S3. Both sequences S2 and S3 are composed of two different facies (See Figure 2.1).

Based on this schematic illustration, a reference model was generated using SIS on the field at a fine resolution with the following variograms for the five different facies:

$$\gamma_1(\mathbf{h}) = 1.0\ Sph_{\substack{ah\_\max=1500 \\ ah\_\min=1000 \\ avert=5}}(\mathbf{h})$$

$$\gamma_2(\mathbf{h}) = 1.0\ Sph_{\substack{ah\_\max=900 \\ ah\_\min=180 \\ avert=5}}(\mathbf{h})$$

$$\gamma_3(\mathbf{h}) = 1.0 Sph_{\substack{ah\_\max=900 \\ ah\_\min=180 \\ avert=5}}(\mathbf{h})$$

$$\gamma_4(\mathbf{h}) = 0.05 + 0.95\ Sph_{\substack{ah\_\max=1000 \\ ah\_\min=500 \\ avert=5}}(\mathbf{h})$$

$$\gamma_5(\mathbf{h}) = 0.05 + 0.95\ Sph_{\substack{ah\_\max=1000 \\ ah\_\min=500 \\ avert=5}}(\mathbf{h})$$

where the $\gamma_i(\mathbf{h})$ is the variogram model corresponding to the i^{th} facies, and *ah_max* is the range in the maximum continuity direction (in this case, north), and *ah_min* is the range in the minimum continuity direction (east), and *avert* is the range in the vertical direction. For image cleaning purposes, the resulting model was then post-processed

using a maximum a-posteriori selection (`maps`) program (Deutsch, 1998). Figure 2.2 shows a 3-D view of the reference model.

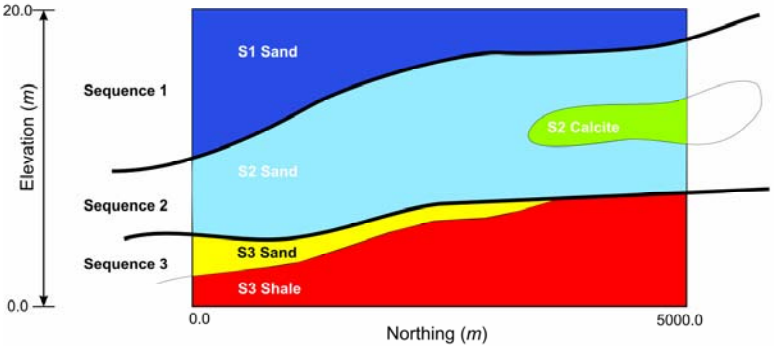

Categories	Code
Sand in Seq. 1	1
Sand in Seq. 2	2
Lime in Seq. 2	3
Sand in Seq. 3	4
Shale in Seq. 3	5

Figure 2.1 Schematic illustrations of three different sequences consisting of five facies exist in the field of study and their corresponding codes.

Suppose that six wells are sampled and the declustered facies proportions are recorded. Figure 2.3 shows the well locations and the declustered histogram of facies. Using these six wells and the declustered proportions, indicator kriging is performed on the full field for a grid size of 10m in easting, 25m in northing and 15m in elevation (for a total of 400000 blocks).

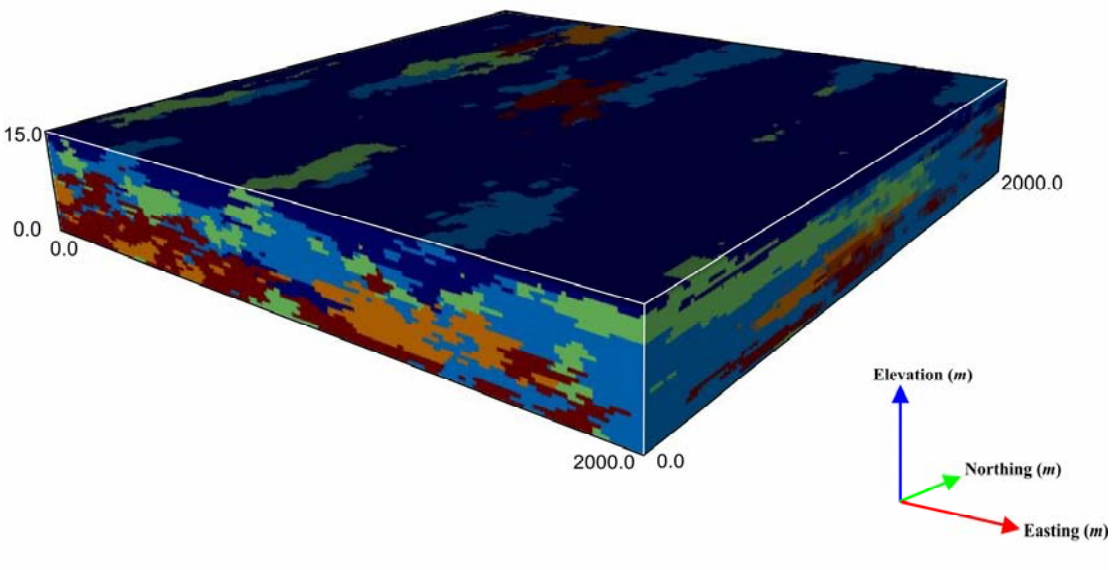

Figure 2.2 3-D reference model generated by SISM.

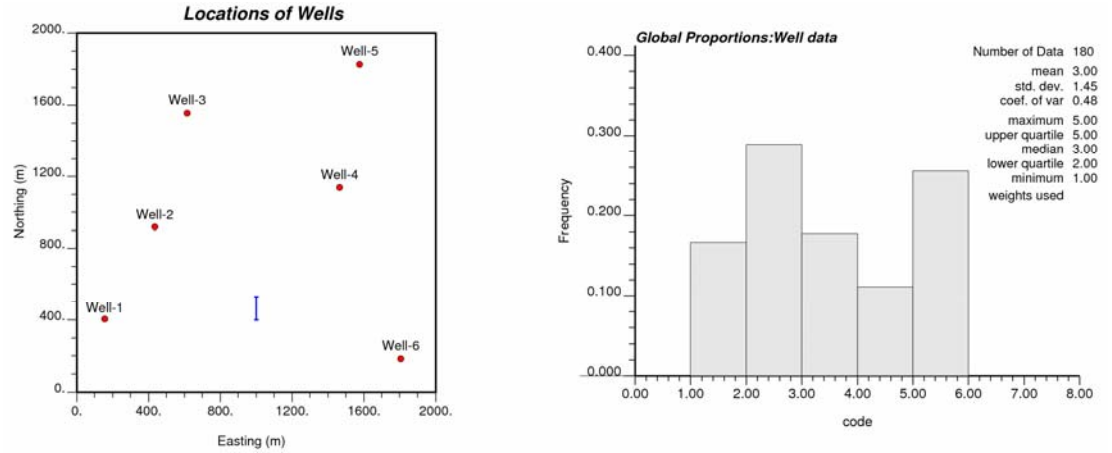

Figure 2.3 Location of sample wells in the field (left) and declustered histogram of facies proportions from well data (right).

For the purpose of a refined geological heterogeneity description, five blocks at a northing-elevation cross section is arbitrarily chosen at an Easting of 1000*m* and a Northing between 400 and 525*m*. This is sufficiently far away from the available wells and little to no local information is available. Figure 2.4 shows the cross section of the reference model at X=1000 *m* (where X is aligned in the easting direction).

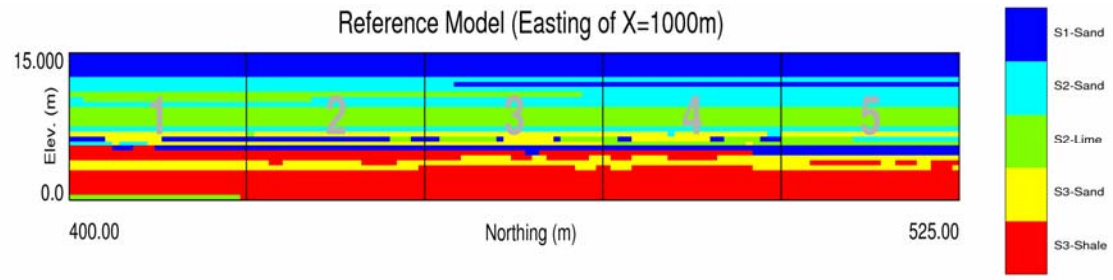

Figure 2.4 Cross section at easting of 1000*m* showing the five arbitrarily chosen blocks for local refinement of the geology model.

As we proceed with applying indicator simulation for local refinement, two issues are considered for detailed analysis: local grid discretization and the simulation order of the five blocks. For the first issue of grid discretization, we consider simulation of only the first block centered at a northing of 412.5*m*. Three different grids are examined: 50 x 30 cells (for a cell size of 0.50*m* x 0.50*m*), 50 x 60 cells (for a cell size of 0.50*m* x 0.25*m*), and 100 x 60 cells (for to a cell size of 0.25*m* x 0.25*m*). Figure 2.5 shows simulated and reference block 1 with three different grid sizes. Of the three examined grids, the result with 50 x 60 cells appears to show relatively good agreement with the reference model and is a good compromise between the coarse results of the 50 x 30 cell grid and the noise from the 100 x 60 cell grid. Using very fine cells is not efficient especially for the cases that we deal with many coarse scale blocks.

In order to check the sensitivity of results on the block simulation order two different block simulation orders are examined; (a) regular path from left to right (1,2,3,4 and 5) and (b) random path (1,3,5,2 and 4). For the case (a) block 1 is simulated first using the surrounding well data and then the adjacent block (block 2) is simulated using well data plus simulated values from the previous block. Five connected blocks are simulated sequentially with the same method. In case (b) we have conditioning data from both sides (not only from left side). Block 1, 3 and 5 are simulated with the same method and after that block 2 and 4 are simulated using left and right hand side blocks (block 1 and 3 for block 2, and block 3 and 5 for block 4) plus the well data. Figure 2.6 shows the results for five connected blocks with two different simulation sequences.

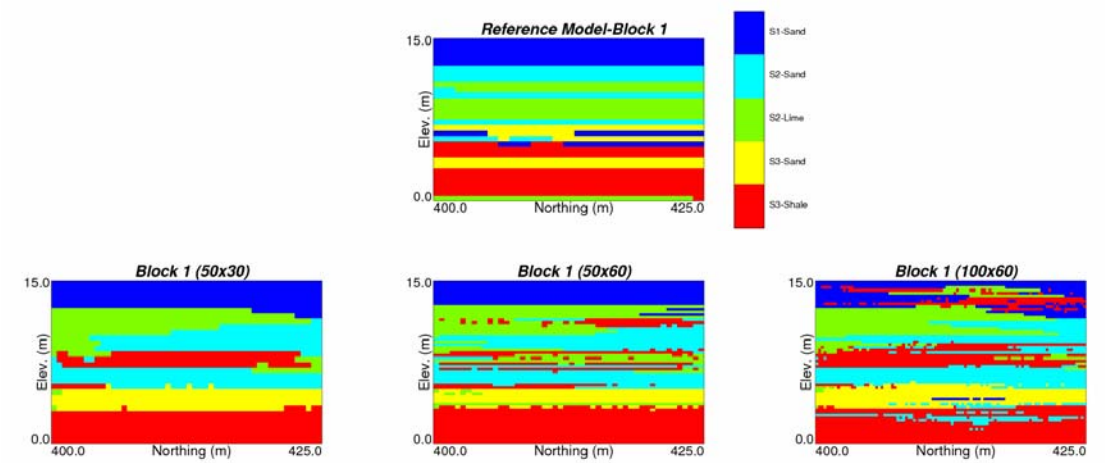

Figure 2.5 Reference (Top) and simulated models of Block 1 (Bottom row) at different grid discretization.

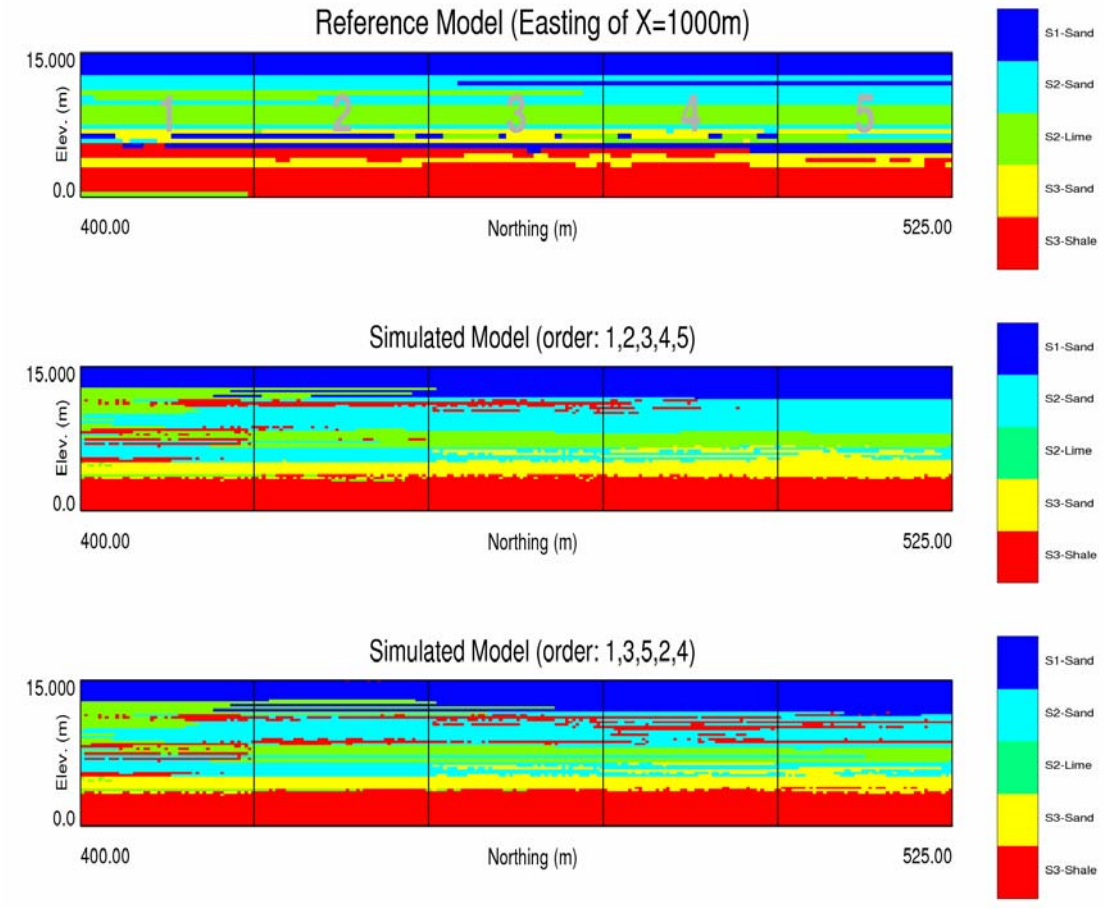

Figure 2.6 Reference model (Top) and Five blocks simulated with order from Left to right (Middle row) and order of 1,3,5,2,4 (Bottom row).

2.4.2 Unstructured Blocks

The same setting as the previous example is considered. For the purpose of a refined geological heterogeneity description, three connected unstructured blocks are considered far away from the available wells. Figure 2.7 shows the location of wells and the unstructured coarse blocks.

Each unstructured block is surrounded by a bounding box and simulated separately. We start from block 1 and then add the results to the well data and proceed to the next blocks. Three simulated blocks are shown in Figure 2.8.

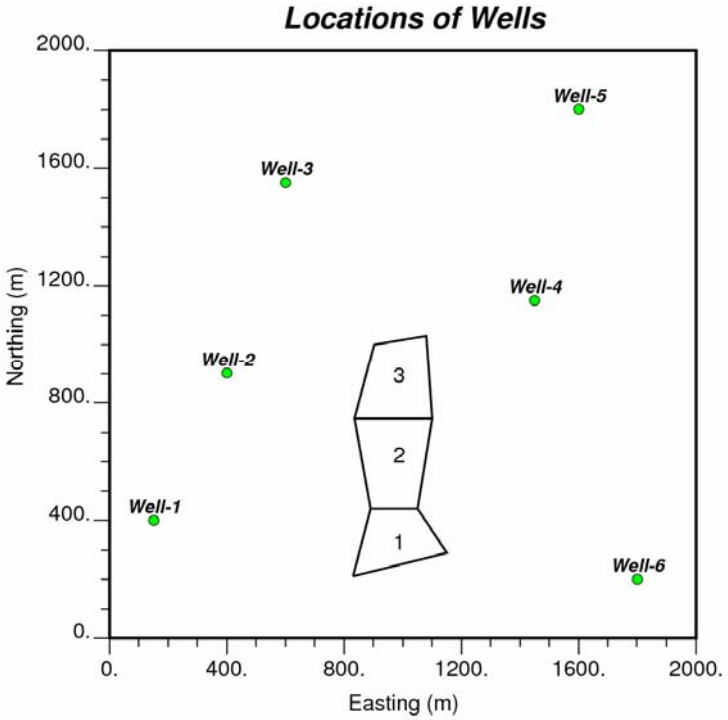

Figure 2.7 Location of wells and the imposed unstructured blocks (left) and the declustered facies proportion (right).

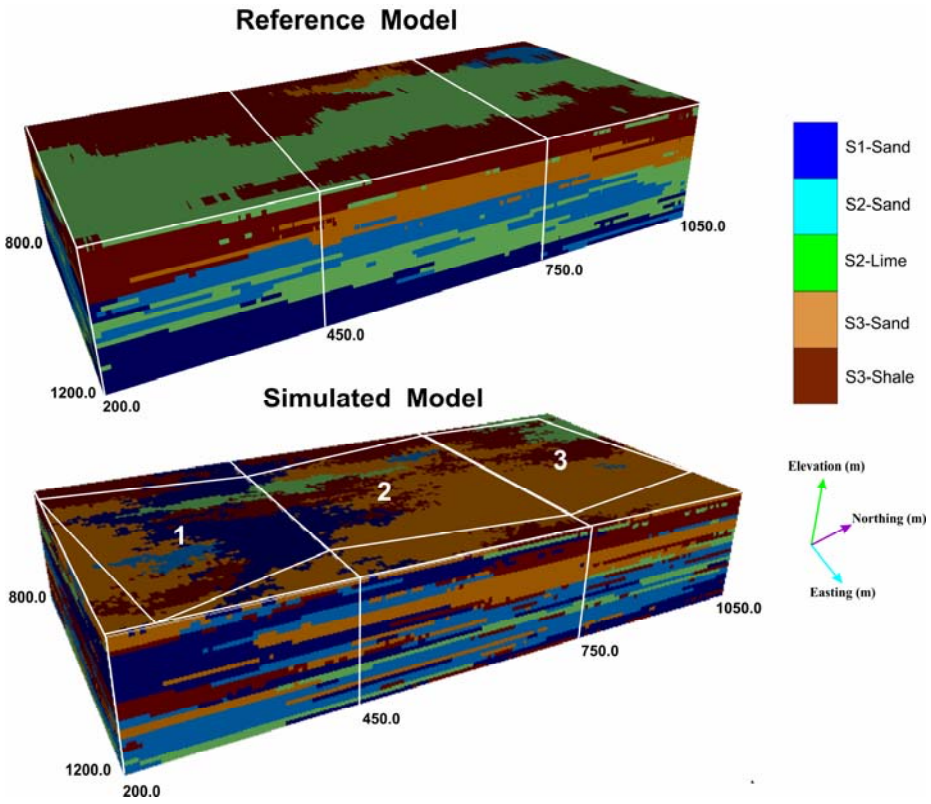

Figure 2.8 Reference model (top) and three connected blocks which are separately simulated (bottom).

2.5 Discussion

Modelling the geological heterogeneity and facies is important in reservoir characterization. Depending on the grid discretization and sequences used in simulation the number of conditioning data increases and this requires more computational time. However this methodology is supposed to be used for large blocks and there is no need to implement it on small grids where internal facies connectivity is not so important. Here the issue would be to select the big blocks to be refined. This is very subjective and mainly depends on the practitioner judgment. One idea is to define a volume threshold and pick the blocks with volume greater than that threshold. The threshold can be a function of many factors such as dispersion variance of point scale data and block scale, block volume and etcetera.

Choosing block simulation path is another important factor. According to the synthetic example in section 2.4.1, there is no significant difference between the results of two regular and random paths which were used for simulation. However, the random path is preferred to the regular path because in the regular path the conditioning data are always from one side (left side for example in section 2.4.1) and this can results in artifacts (McLennan, 2002).

Facies ordering may be more important in some special cases. Using truncated Gaussian simulation or even truncated pluri-Gaussian simulation are alternatives to sequential indicator simulation and may yield better results.

Chapter 3 : Permeability Tensor Upscaling for Unstructured Grid Block

In the case of a homogeneous permeability field, rock permeability is considered as a constant value in any direction. However, real reservoir rocks exhibit heterogeneity at different scales. Due to this heterogeneity, the rock permeability is direction dependent and presented as a tensor. The permeability tensor is needed to correctly solve the flow equation in heterogeneous cases. This becomes more important when unstructured blocks are used in flow simulation problems because the unstructured blocks are generally not aligned to the principal directions of flow.

In this chapter, a brief review of available permeability upscaling is presented and then the proposed methodology is described. Some sensitivity analyses are also presented.

3.1 Background

Permeability upscaling refers to a procedure in which the underlying fine scale permeability is averaged up, to return the effective permeability of a larger domain. There are several upscaling techniques available in the literature. These techniques are generally divided into two main categories: direct method and flow-based method. The direct method is based on the simple averaging of heterogeneous permeability within the coarse block. However, in flow-based upscaling the coarse block’s permeability is calculated based on the solution of flow equation. Depending on the complexity of the problem and the level of accuracy required, both methods can be applied.

In an ideal case, the simple averaging methods are fast and easy to implement. For example, the equivalent permeability for a group of fine grids serially arranged has been analytically proven to be equal to their harmonic average. If the blocks are arranged in parallel to the flow direction, the equivalent permeability is equal to their arithmetic average (see Figure 3.1) (Deutsch, 1987; Kelkar and Perez, 2002). These two basic cases are the worse and the best case of connectivity in the direction of flow, respectively.

Arithmetic and harmonic averages are the upper and lower limits for calculated block permeability, respectively (Cardwell and Parsons, 1945). Journel et. al. (1986), Deutsch (1989) and Desbarats and Dimitrakopoulos (1990) showed different applications of power averaging in estimation of equivalent block permeability:

$$k_V = \left[\frac{1}{V} \int_V k_\omega^p (\mathbf{u}) \right]^{\frac{1}{p}}$$

where k_V is the coarse block permeability, V is the coarse block volume, k_ω is fine scale permeability and $p \in [-1,1]$ depends on the number of factors such as heterogeneity at small scale, the block shape and flow conditions inside the block.

King (1989) used the renormalization technique to compute the block permeability. In this method the upscaling starts from a small block and the size of block is increased successively until the flow simulation block size is reached. This method is very fast and simple but it does not work very well in highly anisotropic media.

For more complex cases with increasing heterogeneity, flow-based upscaling techniques yield more accurate results. In this type of upscaling the flow equation is solved for pressure and the results are used to obtain the block permeability. Choosing appropriate boundary conditions is very important in flow-based upscaling. Figure 3.2 shows examples of boundary conditions which are commonly used in the literature. Warren and Price (1961) applied this technique with constant pressure and no-flow boundary conditions for regular coarse blocks to obtain the diagonal tensor.

Usually cases that involve the use of irregular block or a heterogeneous permeability field at fine scale require calculation of the full permeability tensor. White and Horne (1987) were the first to propose a technique to fully determine non-diagonal block permeability tensors. They used different sets of boundary conditions and solved the flow equation for the entire field of study. The resulting block permeability tensors are neither always symmetric nor positive-definite. Gomez-Hernandez (1994) used many linear boundary conditions and solved the flow equations over an area comprising the coarse block and a skin region. They calculated the full tensor for regular coarse blocks. Durlofsky's (1991) idea of periodic boundary returns symmetric and positive definite full permeability tensor in a medium with periodic condition (for example, repetitive geological structures).

Almost all of the above mentioned techniques are applied on regular blocks. Tran (1995) proposed a method in which the pressure is calculated in the smallest rectangle that includes the irregular block. However, the calculated permeability is diagonal. He (2000 and 2004) applied Durlofsky's periodic boundary condition and solved the flow equations with a finite element method for general quadrilateral grid blocks. This method gives the same accuracy as finite difference method in 2-D quadrilateral blocks but it is not efficient for 3-D blocks. Prevost (2003) implemented both permeability and transmissibility upscaling on general 3-D blocks and showed that the transmissibility upscaling is generally more accurate, but it is time consuming because the flow equation must be solved for all block interfaces.

In this thesis, a new approach is introduced for calculation of permeability tensor for corner point unstructured grid block. This method is based on the finite difference discretization and an optimization technique. The random boundary conditions are used instead of conventional boundary conditions. The following sections describe the methodology in more detail.

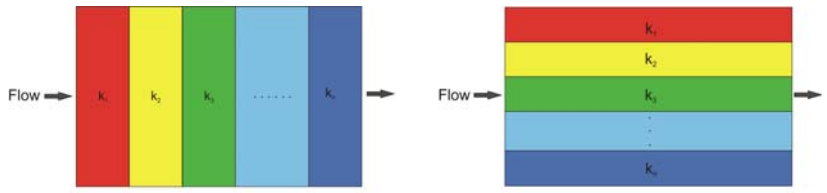

$$k_{eff} = \frac{n}{\sum_{i=1}^{n} \frac{1}{k_i}} \qquad k_{eff} = \frac{1}{n} \sum_{i=1}^{n} k_i$$

Figure 3.1 Upscaled effective permeability for simple cases of serial (left) and parallel (right) layers. Redrawn from Kelkar and Perez (2002).

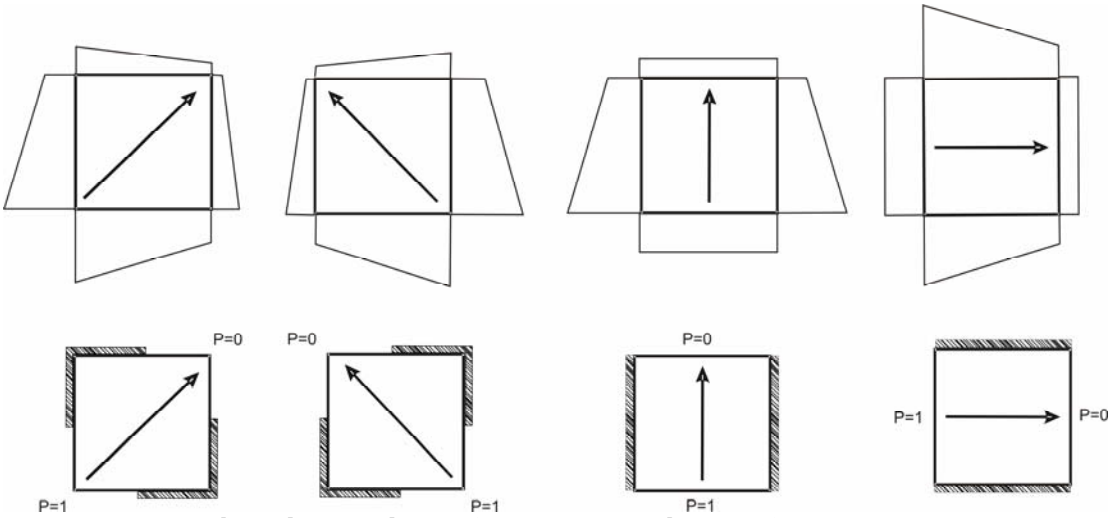

Figure 3.2 Linear boundary conditions (Gomez-Hernandez, 1994) in top row, constant pressure and no-flow boundary conditions (White and Horne, 1987) in bottom row. Hatch lines show the no-flow faces.

3.2 Proposed Methodology

Flow based upscaling technique is used to calculate effective permeability of coarse block. Consider single rectangular block (2-D) or a regular box (3-D) imposed on a fine scale uniform Cartesian grid (See Figure 3.3). The idea here is to calculate the pressure at fine scale with specific boundary conditions applied at the boundary of the coarse block and then use this solution to calculate the permeability tensor for the coarse block. The work flow for permeability upscaling is shown at the end of this chapter.

3.2.1 Random Boundary Condition

As discussed earlier in the previous section, flow boundary condition is a key factor in the calculation of permeability tensors. To obtain a robust and realistic permeability tensor, general linear boundary conditions are considered here.

In this technique four pressures in 2-D (or eight pressures in 3-D) are randomly assigned to the corners of the coarse block. In 2-D, the pressure gradient at each edge is considered to change linearly between the pressures at the two adjacent corners. In 3-D, each face will have a different pressure distribution, defined by using different pressures at the four corners and applying a bilinear interpolation. This provides a smooth map of pressure at six sides of a 3-D coarse block (See Figure 3.4).

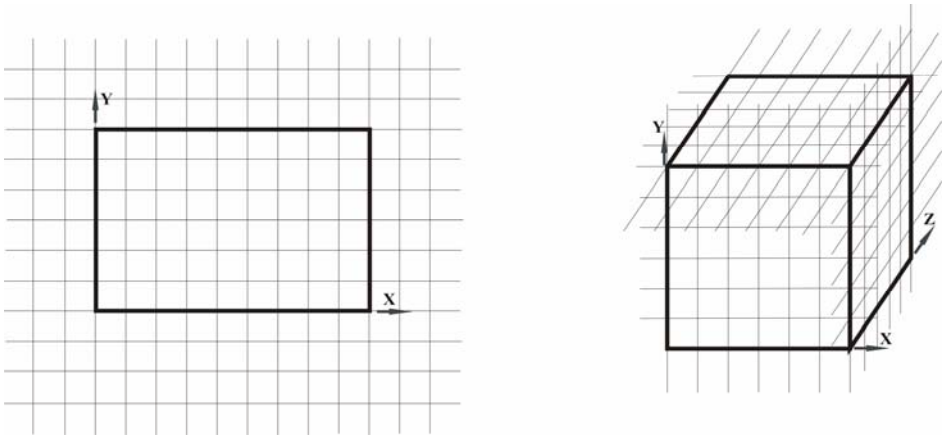

Figure 3.3 Regular coarse blocks imposed on 2-D and 3-D fine scale grids.

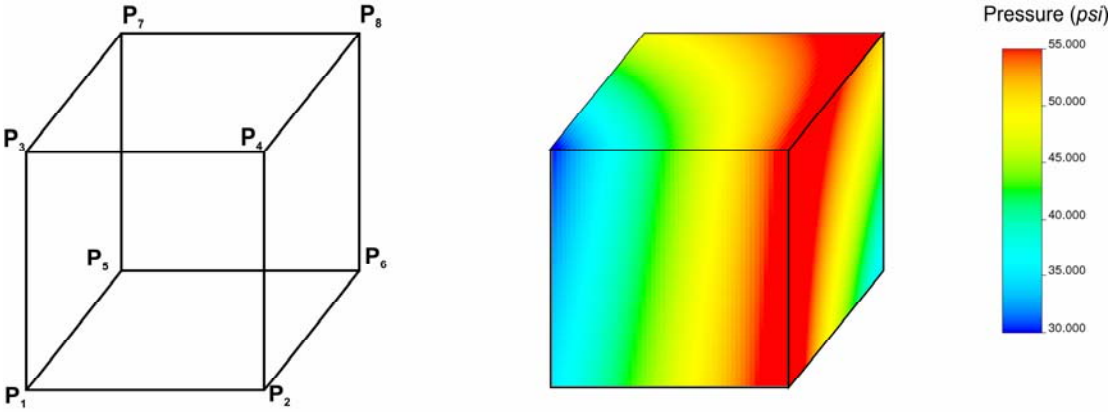

Figure 3.4 Eight pressures are randomly assigned to the corners (left) and the pressure distribution is generated by bilinear interpolation (right).

3.2.2 Flow Equation

Once the boundary conditions are assigned, the flow equation is solved for all fine grids inside the coarse block. The single phase steady state flow equation with the assumption of incompressible fluid and rock is considered:

$$\frac{\partial}{\partial x}\left(k_x \frac{\partial P}{\partial x}\right)+\frac{\partial}{\partial y}\left(k_y \frac{\partial P}{\partial y}\right)+\frac{\partial}{\partial z}\left(k_z \frac{\partial P}{\partial z}\right)=0 \tag{3.1}$$

where P is the pressure, and k_x , k_y and k_z are the fine scale permeability in x, y and z direction, respectively.

The next step is to calculate the average pressure differences and flow rates. The pressure differences are determined by calculating the average of all fine scale pressures over the coarse block volume:

$$\begin{aligned}
\Delta p_x &= \frac{1}{n_{tot}} \sum_{k=1}^{n_z} \sum_{j=1}^{n_y} \sum_{i=2}^{n_x} \left(p_{i,j,k} - p_{i-1,j,k} \right) \\
\Delta p_y &= \frac{1}{n_{tot}} \sum_{k=1}^{n_z} \sum_{i=1}^{n_x} \sum_{j=2}^{n_y} \left(p_{i,j,k} - p_{i,j-1,k} \right) \\
\Delta p_z &= \frac{1}{n_{tot}} \sum_{j=1}^{n_y} \sum_{i=1}^{n_x} \sum_{k=2}^{n_z} \left(p_{i,j,k} - p_{i,j,k-1} \right)
\end{aligned} \tag{3.2}$$

The flow rates are the volume average of flow rates between the fine scale points:

$$\begin{aligned}
Q_{actual-x} &= \frac{1}{n_{tot}} \sum_{k=1}^{n_z} \sum_{j=1}^{n_y} \sum_{i=2}^{n_x} T_x^{i-1/2,j,k} \cdot \left(p_{i,j,k} - p_{i-1,j,k} \right) \\
Q_{actual-y} &= \frac{1}{n_{tot}} \sum_{k=1}^{n_z} \sum_{i=1}^{n_x} \sum_{j=2}^{n_y} T_y^{i,j-1/2,k} \cdot \left(p_{i,j,k} - p_{i,j-1,k} \right) \\
Q_{actual-z} &= \frac{1}{n_{tot}} \sum_{j=1}^{n_y} \sum_{i=1}^{n_x} \sum_{k=2}^{n_z} T_z^{i,j,k-1/2} \cdot \left(p_{i,j,k} - p_{i,j,k-1} \right)
\end{aligned} \tag{3.3}$$

where $n_{tot} = n_x \times n_y \times n_z$ and $T_x^{i-1/2,j,k} = 2 \times \frac{k_x^{i-1,j,k} \times k_x^{i,j,k}}{\left(k_x^{i-1,j,k} + k_x^{i,j,k}\right)} \times \frac{\left(\Delta y \times \Delta z\right)}{\Delta x}$ is the transmissibility term.

3.2.3 Optimization

Applying many different boundary conditions and having sets of pressure differences and flowrates, we can fit a tensor with the minimum error using an optimization technique. In this technique we start with an initial assumed tensor. The predicted flow rates (Q_x^*, Q_y^* and Q_z^*) are calculated using the following general Darcy's law considering an initial permeability tensor and the calculated averaged pressure differences for the first boundary condition:

$$\begin{bmatrix} Q_x^* \\ Q_y^* \\ Q_z^* \end{bmatrix} = -\begin{bmatrix} k_{xx} & k_{xy} & k_{xz} \\ k_{yx} & k_{yy} & k_{yz} \\ k_{zx} & k_{zy} & k_{zz} \end{bmatrix} \cdot \begin{bmatrix} \Delta p_x \\ \Delta p_y \\ \Delta p_z \end{bmatrix} \tag{3.4}$$

An initial objective function (error) is calculated by using the following formula:

$$Obj = \frac{\sum_{B.C.} \sum_{dir} \left\| Q_{actual} - Q^* \right\|}{n_{bc} \times n_{dir}} \tag{3.5}$$

where the inside summation is the flow rate taken over the directions (X,Y and Z), the outside summation is over different boundary conditions, n_{bc} in number of boundary conditions and n_{dir} is number of directions,.

We proceed by proposing a change in tensor and calculating the new objective function. The change is kept if the new objective function is smaller than the previous one. This process is repeated many times until reaching the acceptable error. There is a flexibility to fit full, symmetric or diagonal tensor by adding a simple constraint for the cross terms in tensor to be equal (symmetric) or zero (diagonal).

3.3 Application to Unstructured Block

The methodology discussed above is straightforward for Cartesian grids, but can also be applied to an unstructured block via some simplifying modifications. The coarse irregular block is surrounded by the smallest rectangle (2-D) or smallest box (3-D); consider this as a bounding box (Figure 3.5). We can discretize the irregularly shaped coarse scale block using the underlying fine scale model. This can be easily determined by evaluating whether or not the centre point of a fine scale block falls inside the irregular coarse block. The pressure differences and flowrates are averaged over the fine scale grids that comprise the coarse block. A more accurate approximation to the irregular coarse scale block can be obtained if the underlying heterogeneity model is at a sufficiently fine scale.

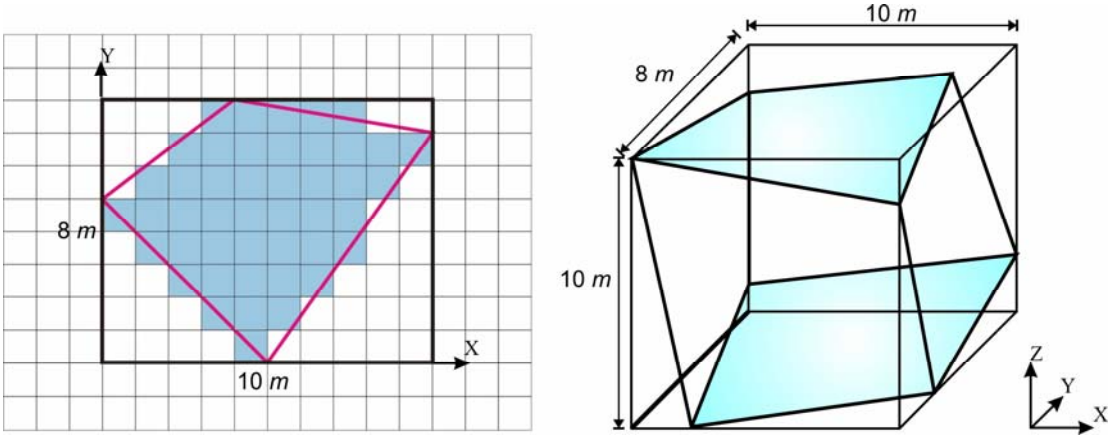

Figure 3.5 Bounding Box around 2-D (left) and 3-D (right) unstructured block. Shaded fine scale blocks lie inside the coarse irregular block are considered for the calculation of effective permeability.

In 2-D cases, any polygonal shape can be easily handled. For 3-D cases, corner point geometry is considered. The unstructured block is defined by two sets of corner points which indicate the upper and lower planes. Both upper and lower planes should have the same number of vertices in a way that each corner point in the upper plane has the corresponding points in the lower plane. Two upper and lower planes are considered to be connected by planar surfaces. The grid blocks are not necessarily aligned vertically and can be tilted in some direction to conform to geologic structures. Figure 3.6 shows examples of this corner point block.

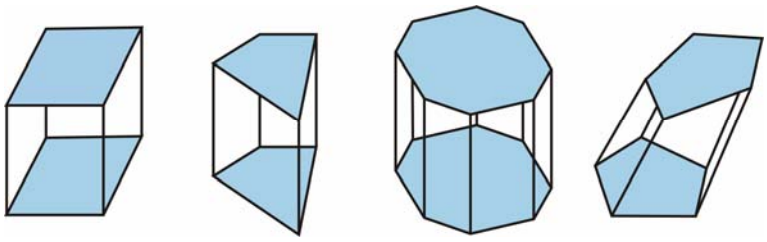

Figure 3.6 Example of corner point structured (left) and unstructured blocks (other). The areal cross section is a convex polygon.

3.4 Sensitivity Analysis

The permeability tensor calculated by flow based upscaling techniques is non unique and depends on many factors, such as the flow boundary condition, size of bounding box, the fine scale permeability assigned to the buffer zone, the geological features inside the coarse block and the orientation of grid block. Indeed, there is an ambiguity about the type of permeability tensor (full, symmetric or diagonal). These factors are described in more detail in the following sections:

3.4.1 Number of Flow Boundary Conditions

It has been shown (Gomez-Hernandez, 1994 and White et. al., 1987) that the block effective permeability not only depends on the fine scale heterogeneity but also on the flow boundary conditions. Different pressures at the boundary impose different flow regimes inside each block and this affects the value of permeability which is numerically calculated or experimentally measured. This becomes more important when considering the permeability tensor which has cross-flow terms. Generally, linear pressure gradient and no-flow boundaries are considered. However, this is not what realistically happens in a reservoir. In this work we considered random pressures assigned at the corner of coarse block so that flow may not be imposed in a specific direction and this will help to appropriately capture the effect of cross-flow in the coarse block. Since many different boundary conditions are needed for this method, the minimum number of boundary conditions required to get a stable permeability tensor is an issue. This can be approximately determined by the following example.

In this example we considered a synthetic permeability model with a single 3D block imposed on it. Ten different permeability realizations are generated by SGSIM (Sequential Gaussian Simulation) at resolution of 100x100x20 (1m x 1m x 1m cell size). Model are considered as the fine scale permeability in X and Y direction (k_x and k_y). The permeability in Z direction is considered multiple of k_x by a constant factor (e.g. $k_z = 0.1 \times k_x$).

Different block shapes are examined. Figure 3.7 shows the permeability models and the irregular blocks. The full permeability tensor is calculated for different numbers of random boundary conditions varying from 3 to 50. Variation of permeability tensor and the minimum error are compared with the number of boundary conditions. Figure 3.8 shows the variation of permeability tensor components and error with the number of boundary conditions for realization 8. As we can see in the figure the tensor components are stable for approximately 10 boundary conditions.

In order to find the minimum number of boundary conditions for each case, the stabilizing criterion is defined as follows:

$$\sum_{i=1}^{3}\sum_{j=1}^{3}\left|\frac{k_{i,j}^{l} - k_{ref_{i,j}}}{k_{ref_{i,j}}}\right| < 1\% \qquad l = 3,....,50 \qquad (1.1)$$

where k is the permeability tensor, i and j indicate the row and column of the permeability tensor and k_{ref} is the tensor calculated for 50 boundary conditions (more stable). The minimum l which satisfies this condition is considered as the minimum number of boundary conditions. Figure 3.9 shows the histogram of the number of boundary conditions calculated for this example. It shows that almost 10 boundary conditions are enough to get stable permeability tensor.

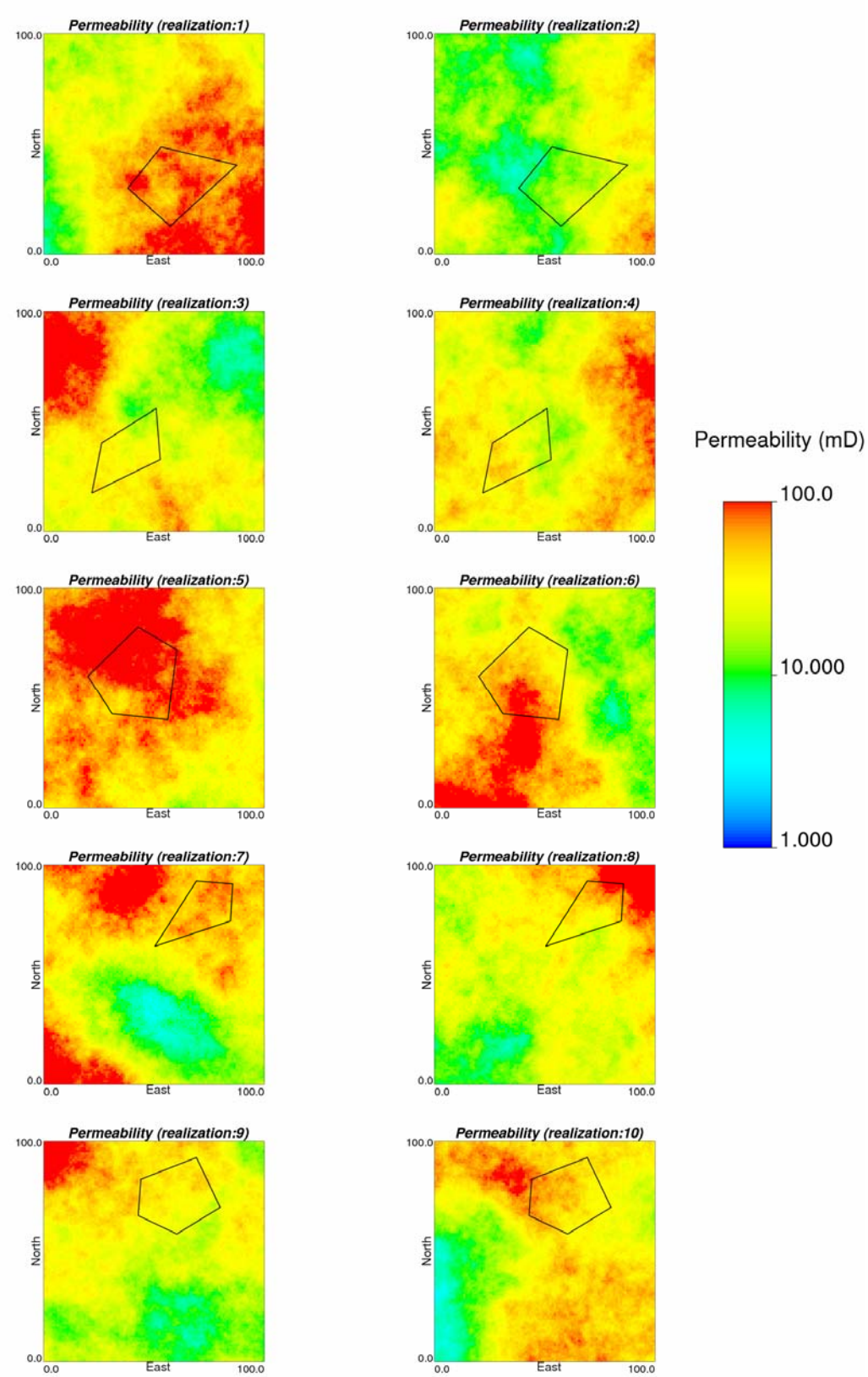

Figure 3.7 Ten permeability realizations with a single unstructured block considered for this example.

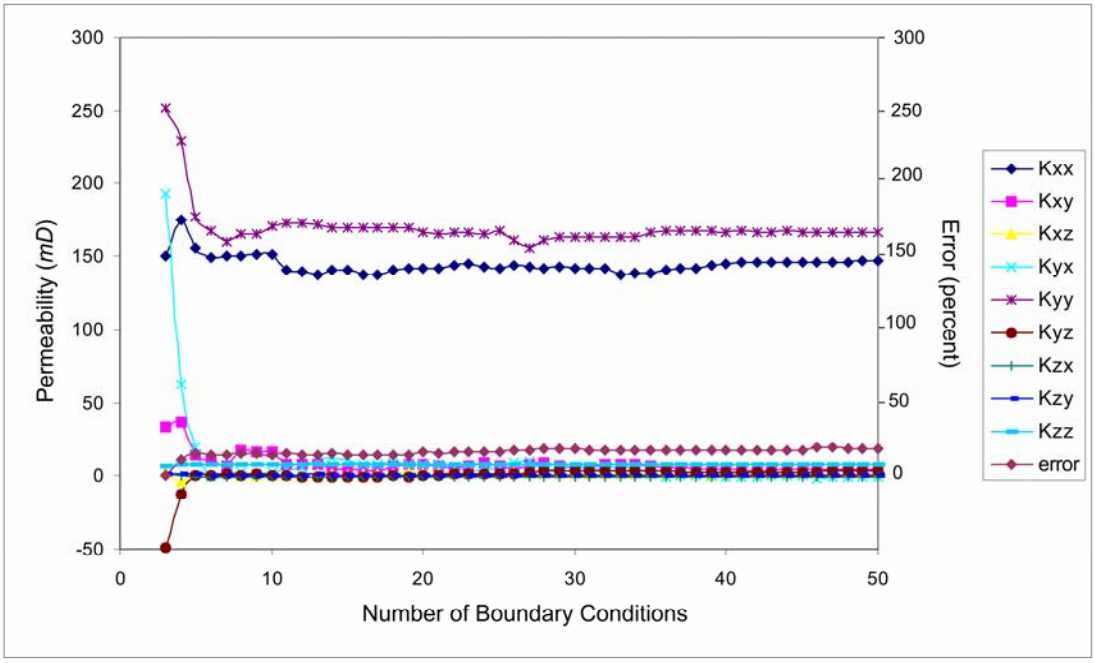

Figure 3.8 Permeability tensor variation with number of random boundary conditions for realization 8.

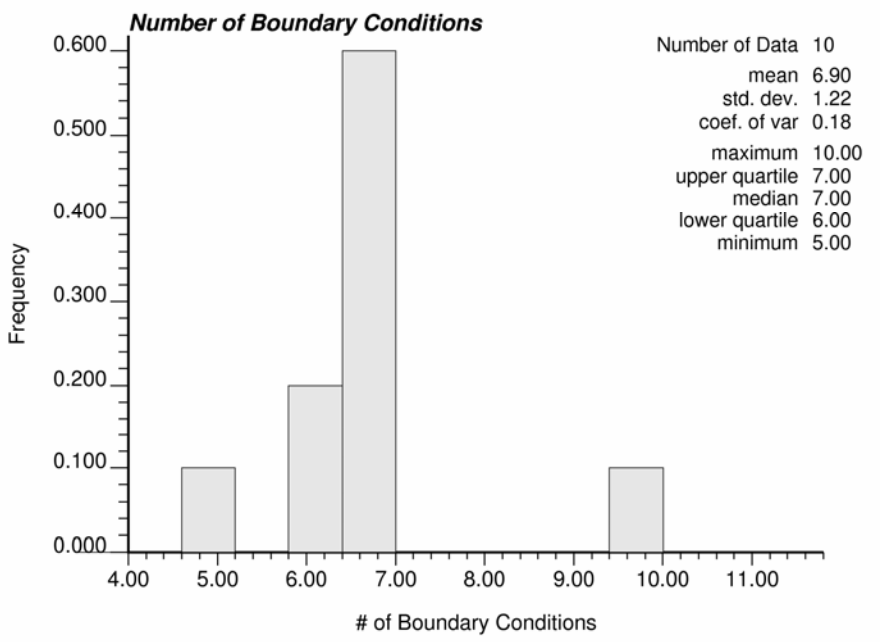

Figure 3.9 Histogram of number of boundary conditions needed for ten different cases.

3.4.2 Bounding Box

In flow-based upscaling the flow equation is usually solved locally for a specific block. Here we consider a bounding box around the unstructured block and solve the flow equation for this box. Two factors may affect the value of the permeability tensor for this case; the size of bounding box and the permeability value assigned to the fine cells inside the bounding box and outside of the irregular block (call this the buffer zone).

To observe the impact of these factors, we generate a 3-D synthetic permeability model (at a resolution of 100 x 100 x 50 grids). A single unstructured block is considered in this field. The bounding box for this block comprises of 20 x 20 x10 fine grids. The full permeability tensor is calculated for the coarse block considering three cases with different bounding box size: (a) 20 x 20 x 10), (b) 40 x 40 x 20 and (c) 60 x 60 x 30 (see Figure 3.10).

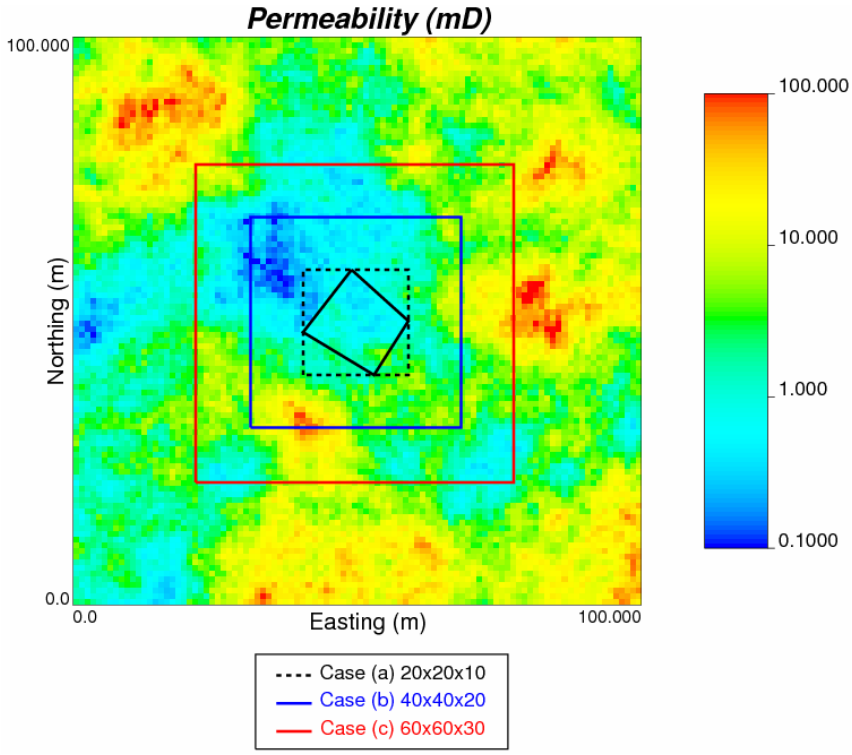

Figure 3.10 Three different bounding box sizes considered for this example.

Consider the case of a heterogeneous buffer zone, Figure 3.11 shows the results of calculating and comparing the diagonal components of the permeability tensor; we see that as the bounding box size increases the main diagonal component of the permeability tensor (k_{xx}, k_{yy}, k_{zz}) decreases slightly, but the error drops significantly. However, if comparing the computing time for these three cases, considering a larger bounding box is inefficient.

In order to check the sensitivity of permeability to the buffer zone permeability, this example is evaluated for a large bounding box (case 3) and homogeneous permeability values of 1, 10, 20, 100 and 500 mD. As Figure 3.12 shows, the permeability tensor calculated for an unstructured block of this example increases as the buffer zone permeability increases. The error also increases systematically as buffer zone permeability increases.

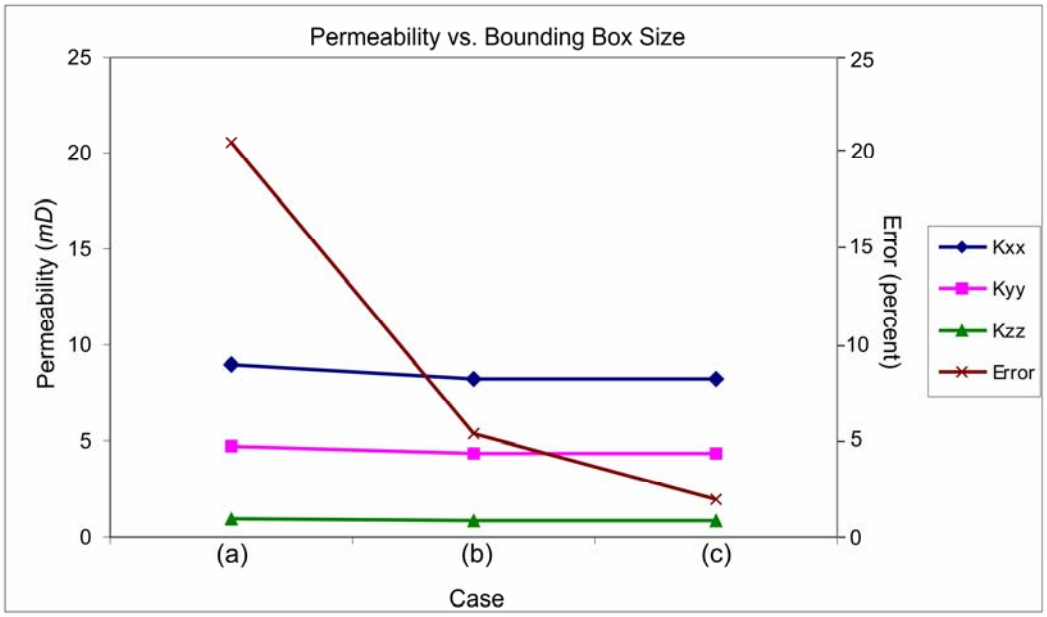

Case	CPU Time (s)
a	3.1
b	12
c	99.27

Figure 3.11 Variation of permeability tensor with bounding box size.

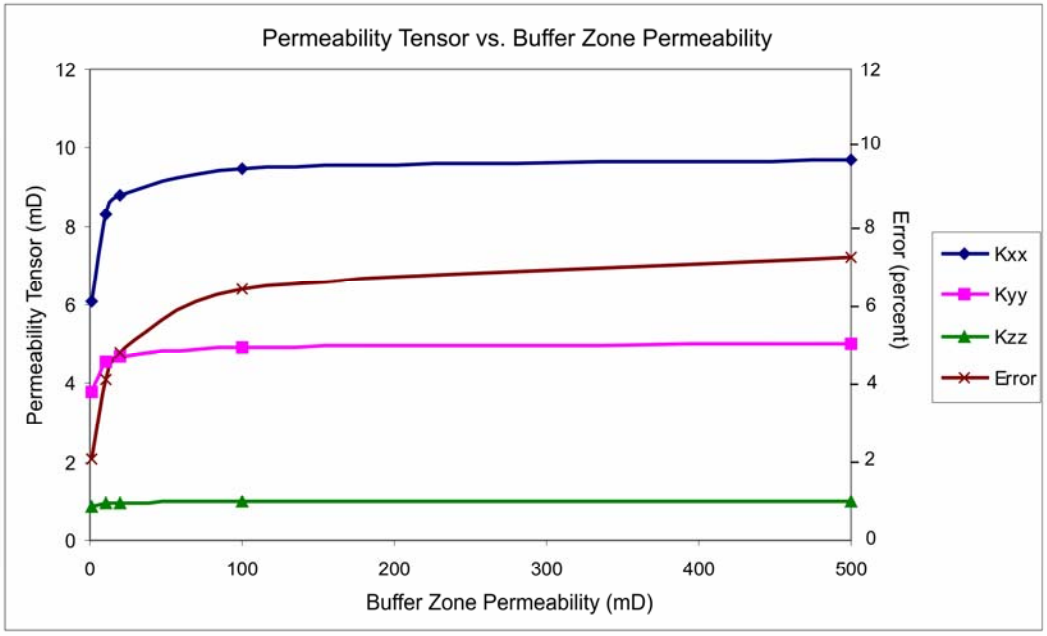

Figure 3.12 Variation of permeability tensor with buffer zone permeability.

3.4.3 Geological Continuity Direction

The fine scale heterogeneity has a significant effect in the coarse block permeability. In some cases the geological features are not aligned with the coarse block sides. This may lead to the appearance of cross flow terms. This is further discussed with the following example.

Consider a single regular block with size of 20*m* by 20*m* imposed in the middle of a field. Sequential Gaussian simulation is run for a square field (100*m* x 100*m* with cells at 1m x 1m resolution) and the permeability is modeled for different continuity directions (0° to 90° azimuth in increments of 5°). An anisotropic variogram with a 70*m* range in the maximum and 10*m* range in the minimum direction is considered. The permeability models are considered as fine scale permeability in both *X* and *Y* directions ($k_x = k_y$; where *X* and *Y* are aligned with easting and northing, respectively). Figure 3.13 shows the permeability models and the single block located at the centre of the field. The full permeability tensor is calculated for each case. As

expected, the permeability in *X* direction increases and the permeability in *Y* direction decreases when the orientation of geological features changes from 0° to 90° azimuth. In order to quantify the variation in the cross-flow terms, we define a cross-flow index as follows:

$$cross\text{-}flow\ index = \frac{\left(k_{xy} + k_{yx}\right)}{\left(k_{xx} + k_{yy}\right)}$$

As we can see in Figure 3.14, the index is smaller when the flow is dominated in the *X* or *Y* direction and this happens when there is more connectivity in those directions.

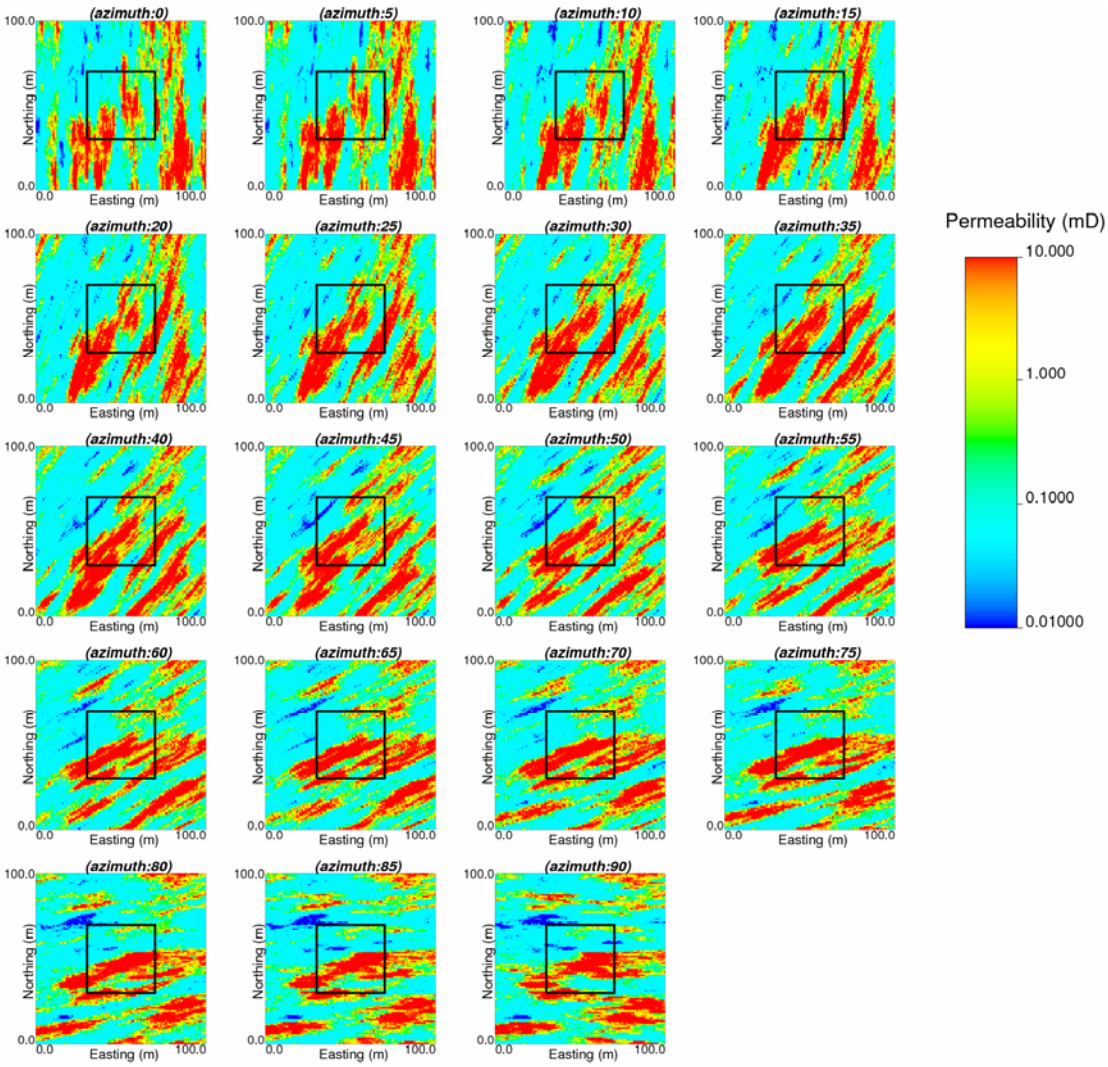

Figure 3.13 Permeability models with different direction of continuity and the location of coarse block.

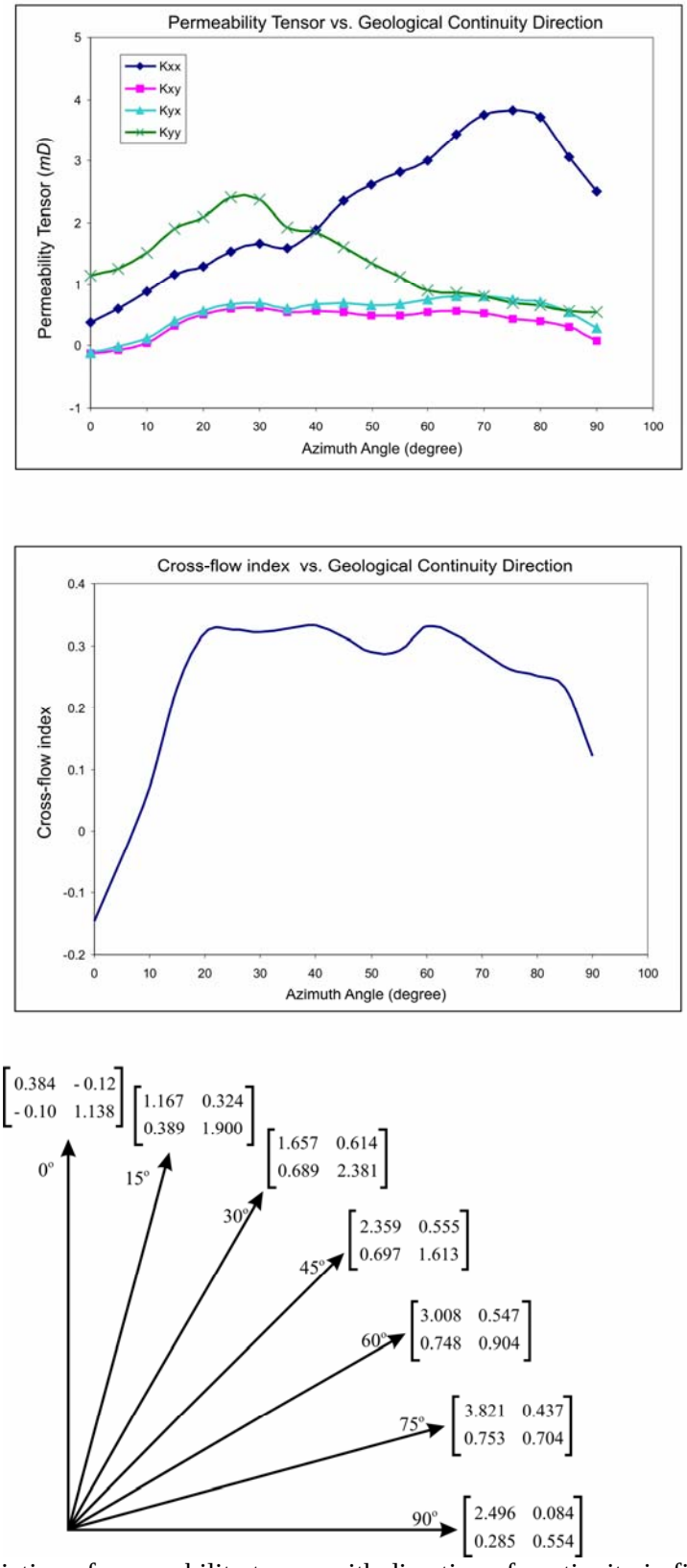

Figure 3.14 Variation of permeability tensor with direction of continuity in fine-scale permeability model.

3.4.4 Grid Block Orientation

In this section the sensitivity of permeability tensor with respect to the block orientation is discussed with an example. A permeability model is selected from the example in section 3.4.3 (with major continuity aligned in 90° azimuth). A single block is imposed in the middle of the field. The block is rotated and the permeability tensor is calculated for each case. Figure 3.15 shows 12 cases with the same permeability model and different block orientations (0° to 360° azimuth in increments of 30°). The permeability tensor for each case is also shown in the Figure 3.15.

The results show that the permeability tensor components changes when the block orientation changes. However, the components do not vary with a specific relation.

3.4.5 Full, Symmetric and Diagonal Permeability Tensor

As discussed in section 3.2.3, fitting a full, symmetric or diagonal permeability tensor is straightforward. The error (objective function) is defined based on the difference between the actual flow rates and the flow rates when the tensor of permeability is considered. In this section we want to show the amount of error introduced when each of the full, symmetric and diagonal permeability is fitted. This can be further investigated with the following example.

The same permeability model and unstructured block as the example in section 3.4.2 is considered with a large bounding box (60x60x30) and 20 random boundary conditions. The full, symmetric and diagonal permeability tensors are fitted. The results are shown in Figure 3.16.

The results show that the full tensor introduces a fitting error of less than 2% (for this example) and the error increases when symmetric or diagonal tensor is fitted. This example reveals the fact that using full permeability tensor returns the flowrates which are more similar to the actual flowrates.

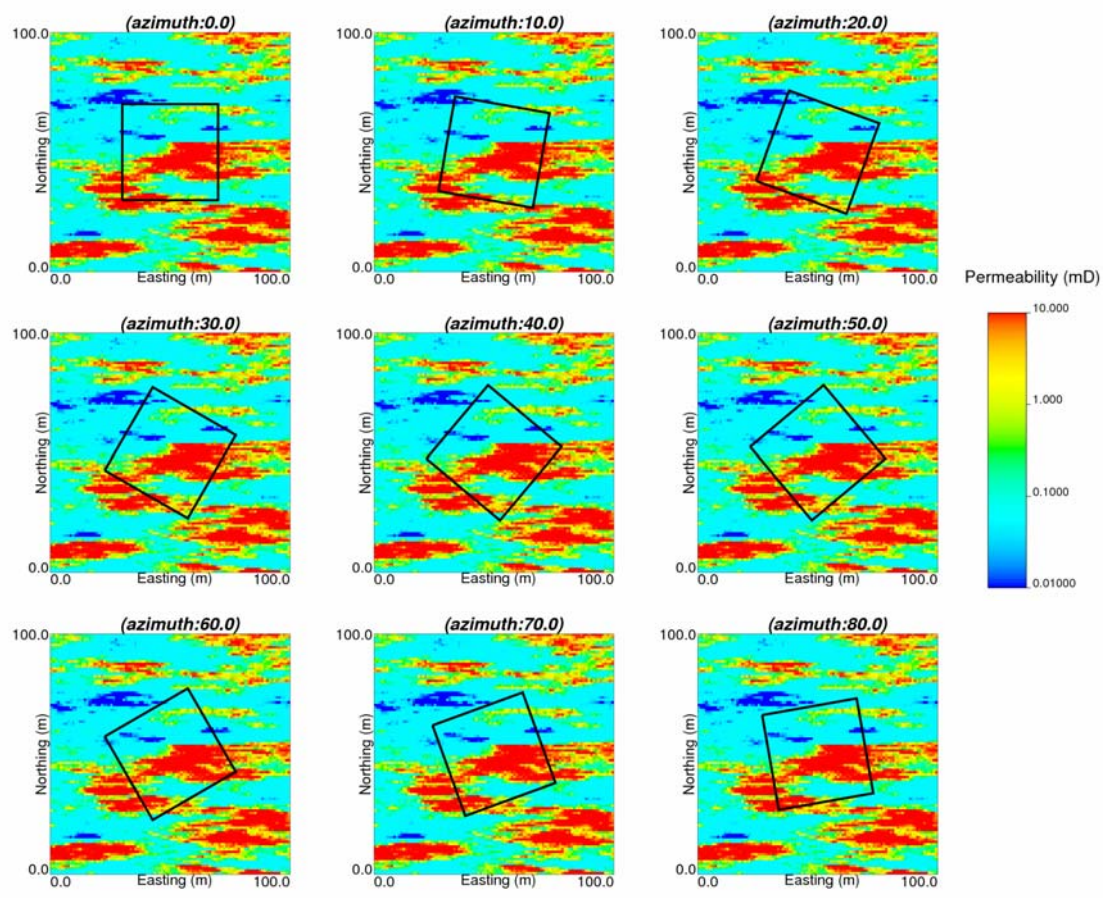

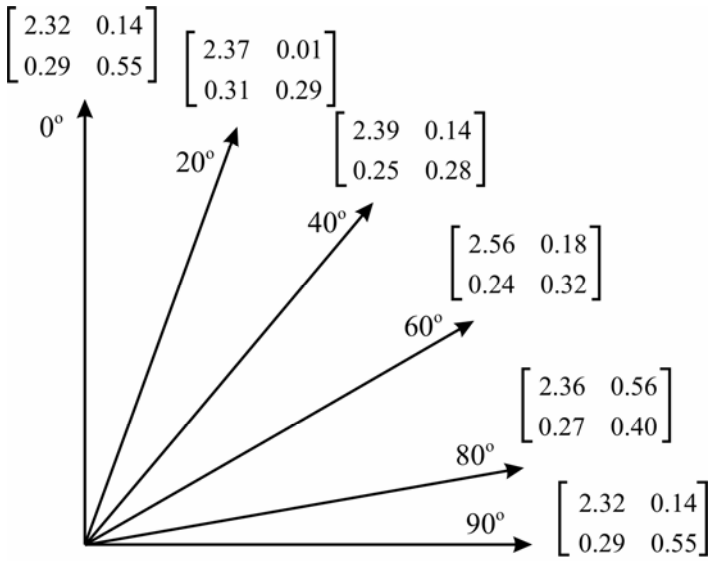

Figure 3.15 Variation of permeability tensor with grid block orientation.

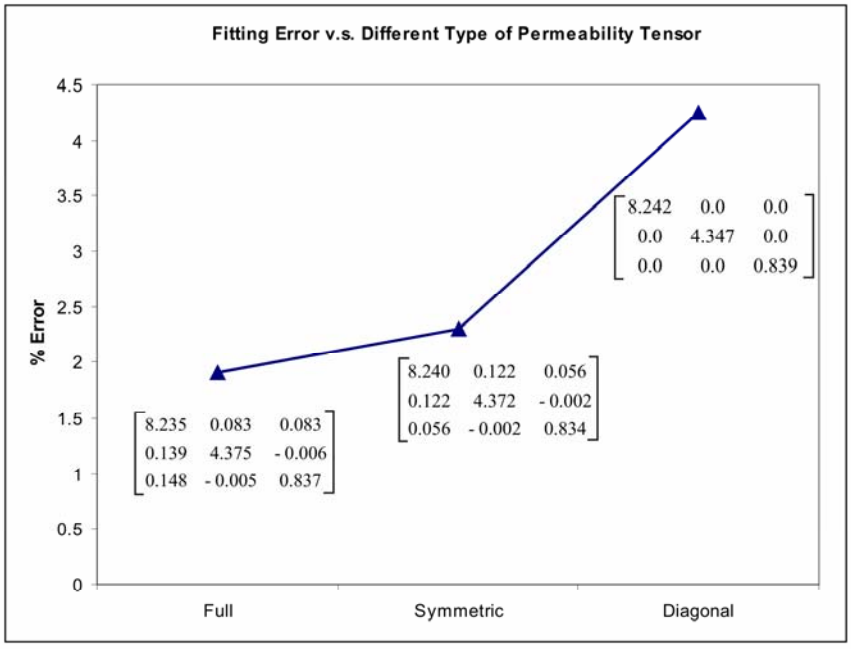

Figure 3.16 Fitting error for full, symmetric and diagonal permeability tensor.

3.5 Discussion

A flow-based upscaling technique with sets of random boundary conditions is developed. Sensitivity analysis reveals that the calculated permeability tensor depends on number of random boundary conditions, bounding box size, geological heterogeneity and also the grid block shape and orientation. Minimum 10 sets of random boundary conditions are required to get stable permeability tensor. A relatively large bounding box with heterogeneous permeability value assigned to the buffer zone is recommended. Shape of permeability tensor is still under discussion of researcher. Some researcher believes that the permeability tensor is symmetric (Bear 1972, Gelhar and Axness 1983), other believes that it is not necessarily symmetric and can be asymmetric (Ababou 1988; King 1993). There is evidence that the tensor could be asymmetric with non-linear boundary conditions. Here we showed that fitting the full permeability tensor returns a smaller error in the calculated flow rate compared to the symmetric and diagonal tensor.

Chapter 4 : Determination of Geological Continuity Direction and Unstructured Block Geometry

The geological continuity is a key factor for prediction of fluid flow in reservoir. The geological continuity and variogram continuity are direction dependent (Deutsch, 2002). In Chapter 3 we show that the permeability tensor depends on the geological continuity direction and the grid block orientation. This chapter introduces a new approach to determine the geological continuity direction and orientation of an unstructured grid block by using the moment of inertia tensor.

4.1 Moment of Inertia

The moment of inertia of a rigid body is related to the distribution of the mass throughout the body and quantifies the rotational inertia of a rigid body (Beer at. al., 1988).

$$I = \int_V mr^2 dm \tag{4.1}$$

where m is mass and r is the perpendicular distance from the axis of rotation.

Generally, there are two forms of moment of inertia; scalar form which is used when the axis of rotation is known and the tensor form that summarizes all moments of inertia for different axes of rotation with one quantity.

For a rigid body consisting of N point masses, $m_i \;\; i = 1, \ldots, N$, the 3D moment of inertia tensor are defined as follows:

$$\mathbf{I} = \begin{bmatrix} I_{xx} & I_{xy} & I_{xz} \\ I_{yx} & I_{yy} & I_{yz} \\ I_{zx} & I_{zy} & I_{zz} \end{bmatrix} \tag{4.2}$$

$$I_{xx} = \sum_{i=1}^{N} m_i \left(y_i^2 + z_i^2 \right) \quad , \quad I_{xy} = I_{yx} = \sum_{i=1}^{N} m_i x_i y_i$$

$$I_{yy} = \sum_{i=1}^{N} m_i \left(x_i^2 + z_i^2 \right) \quad , \quad I_{xz} = I_{zx} = \sum_{i=1}^{N} m_i x_i z_i$$

$$I_{zz} = \sum_{i=1}^{N} m_i \left(x_i^2 + y_i^2 \right) \quad , \quad I_{yz} = I_{yz} = \sum_{i=1}^{N} m_i y_i z_i$$

where x_i, y_i and z_i are the distances of point i from the coordinate axes. Here the physical meaning of I_{xx} is the moment of inertia around the *x*-axis when the objects are rotated around the x-axis and I_{xy} is the moment of inertia around the *y*-axis when the objects are rotated around the *x*-axis.

Since the moment of inertia is an anisotropic quantity and presented as a tensor, the principal directions can be determined with the same approach as discussed in section 1.3. Here the principal directions of moment of inertia show the directions in which the rigid body is more closely distributed or less distributed. In this case the major direction is the one that is related to the smaller moment of inertia. This interesting property leads us to determine the major and minor direction of continuity in the geological setting or define the principal direction of an unstructured grid block.

4.2 Direction Determination Through Moment of Inertia

Generally, the directions of continuity in variables are determined prior to geostatistical modelling. A fairly standard approach is to plot the variogram maps and detect the maximum and minimum continuity direction based on the range of variogram. Geological information and interpretations are another source to detect the continuity direction in lithofacies. This process is subjective and requires user

judgment. In cases where we are dealing with a large number of variables and geological facies, applying this method could be frustrating. Moment of inertia tensor can be used to automatically determine the continuity in geological models and geometry of unstructured grid elements.

4.2.1 Geological Models

The correlation indicates the strength and direction of a linear relationship between two random variables, U and V .

$$\rho_{U,V} = \frac{Cov\{U,V\}}{\sigma_U.\sigma_V} = \frac{E\{(U-\mu_U)(V-\mu_V)\}}{\sigma_U.\sigma_V} \tag{4.3}$$

where σ_U is standard deviation of U , σ_V is standard deviation of V , μ_U is mean of U and μ_V is mean of V .

The correlation varies between -1 to 1. Correlation of 1 shows the perfect linear relationship and -1 indicates an inverse linear relationship. The closer the coefficient is to either −1 or 1, the stronger the correlation between the variables. If the variables are independent the correlation is zero.

The correlation map shows the calculated correlation of a data set for different lag **h** and directions. If we consider the correlation as a mass quantity, then the correlation map can be considered as a rigid body and we can find the maximum and minimum direction of continuity analogous to the method used to calculate the principal axes for moment of inertia.

Given any continuous geological variable model or categorical facies model, the following steps allow us to find the direction of continuity:

1. Generate the correlation map for continuous model. For categorical model, each code can be considered as a mass quantity.
2. Calculate the moment of inertia tensor for the point masses according to the *X*, *Y* and *Z* axes pass through the center of mass.
3. Determine the principal direction of continuity using the method in section 1.3.

We verify the method with the following examples.

Examples

Two models are considered and the principal directions are determined. For the first example a continuous model is generated with unconditional sequential Gaussian simulation (SGS) with the azimuth angle of 60° and dip angle of 0°. The correlation map is calculated and plotted for the range of 1/3 of the field size. Figure 4.1 shows the model and the correlation map.

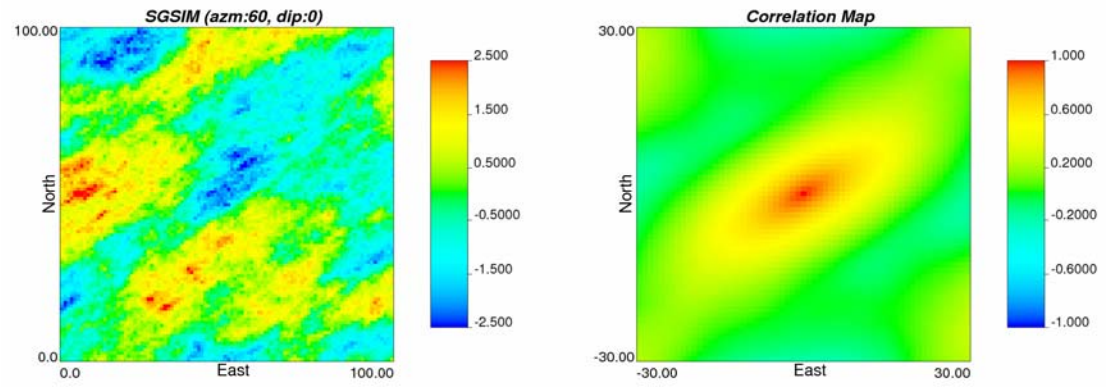

Figure 4.1 A synthetic continuous Gaussian model generated with azimuth of 60° (left) and the calculated correlation map (right).

The moment of inertia tensor is calculated and the principal directions are defined.

$$\begin{bmatrix} I_{xx} & I_{xy} \\ I_{yx} & I_{yy} \end{bmatrix} = \begin{bmatrix} 4514.33 & 4712.47 \\ 4712.47 & 10408.78 \end{bmatrix}$$

$$\tan 2\theta = -\frac{2I_{xy}}{\left(I_x - I_y\right)} \quad \Rightarrow \quad \begin{cases} \theta_1 = 61.01^\circ \\ \theta_2 = -28.99^\circ \end{cases}$$

The major direction is defined by substituting θ_1 and θ_2 into the equation (1.2). The angle with the smaller moment of inertia is the major direction ($\theta_1 = 61.01^\circ$).

$$I_{x'} = \frac{I_x + I_y}{2} + \frac{I_x - I_y}{2}\cos 2\theta - I_{xy}\sin 2\theta \quad \Rightarrow \quad \begin{cases} I_{x'}\left(\theta_1\right) = 5028.69 \\ I_{x'}\left(\theta_2\right) = 9894.42 \end{cases}$$

For the second example a single ellipsoid is generated with the azimuth angle of 20° and the dip angle of 0°. The grids inside the ellipse are coded as 1 and the outside as code 0 (Figure 4.2). The methodology is applied on this model and the inertia tensor is calculated.

$$\begin{bmatrix} I_{xx} & I_{xy} \\ I_{yx} & I_{yy} \end{bmatrix} = \begin{bmatrix} 114976.0 & 53370.0 \\ 53370.0 & 75764 \end{bmatrix}$$

The angles are calculated and the major direction is determined with the same method as last example ($\theta_1 = -69.82^\circ$, $\theta_2 = 21.18^\circ$). The azimuth angle is reproduced with error of 5.8%.

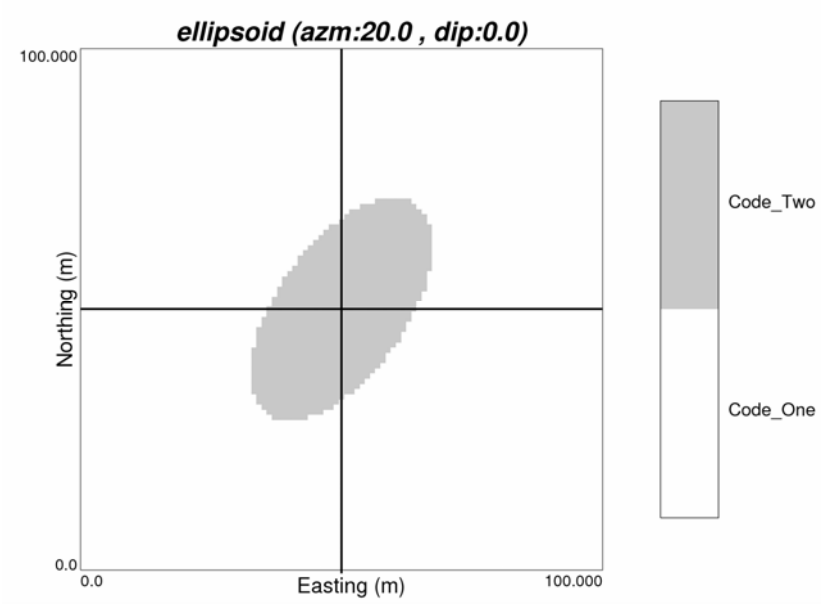

Figure 4.2 A simple categorical example generated with azimuth angle of 20°.

4.2.2 Locally Varying Angles

The anisotropy in the geological setting varies from one point to another due to heterogeneity. In some complex geological setting such as fluvial setting which contains channel features, the continuity direction significantly changes from one region to another. Geostatistical modelling techniques such as sequential Gaussian simulation or sequential indicator simulation with a global variogram orientation and search parameters can not reproduce these local changes in continuity direction. Some attempts have been done to change the simulation algorithms in order to consider the locally varying angles (Leuangthong et. al., 2006).

In the cases where representative training images or other geological model is available, the methodology discussed in section 4.2.1 can be applied locally to determine the local varying continuity direction. This is further explained with the following example.

Example

A 2D training image is considered. The model has 256 cells in both *x* and *y* direction. There are three facies in the model. In order to locally determine the continuity direction a window is considered which contains 16 fine grid cells in *x* and *y* direction. Figure 4.3 shows the training image and the windows which are considered.

A constant value (mass) is assigned to facies type 2 which represents the channels. The mass of other facies are set to 0. The moment of inertia is calculated for each window and the results are plotted in Figure 4.4.

4.2.3 Unstructured Grid Element

The orientation of unstructured grid blocks is an important factor in calculating the upscaled permeability tensor. The upscaling technique discussed in Chapter 3 is based on the fine grid cell permeabilities which are considered for the volume averaging. It is shown in Chapter 3 that for a single unstructured grid block imposed on a specific fine scale permeability model, the upscaled permeability tensor is related to the orientation of unstructured grid block.

The orientation of unstructured blocks can be determined with the same method as discussed in previous section. Each unstructured block is refined locally with the fine Cartesian grid cells and then the inside cells are coded as 1 while the outside cells are defined as code 0. Then the moment of inertia tensor is calculated and the major direction is defined. This is investigated by the following example.

A 2D unstructured grid model is considered. There are 25 grid blocks in this model. Figure 4.5 shows the unstructured grid model. The methodology is applied for each unstructured grid block and the orientation is determined. Figure 4.6 shows the orientation of each grid blocks in the unstructured model.

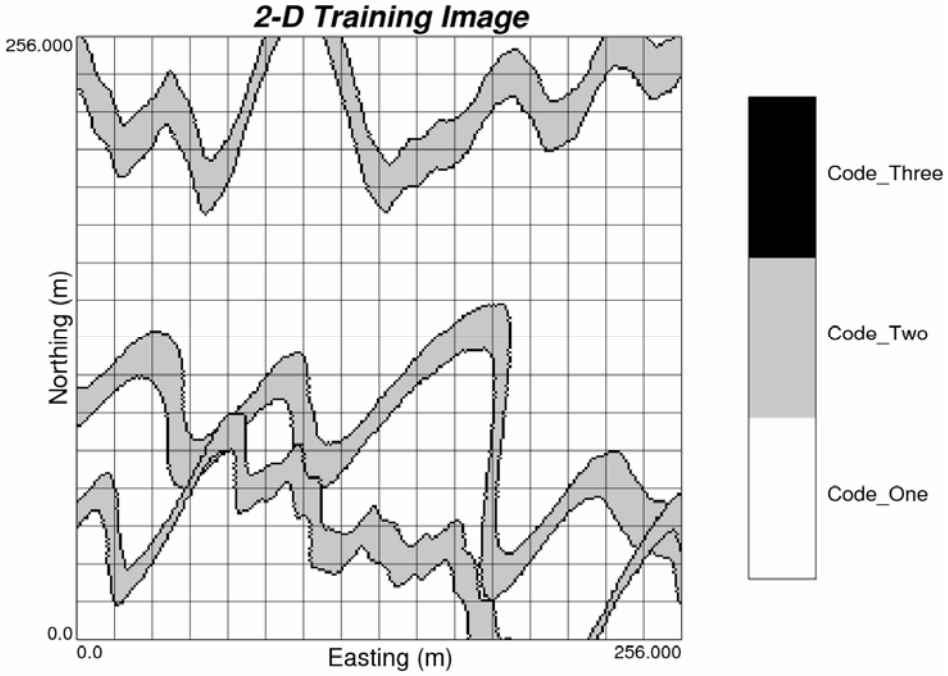

Figure 4.3 The training image considered for determination of locally varying angle. The squares show the windows.

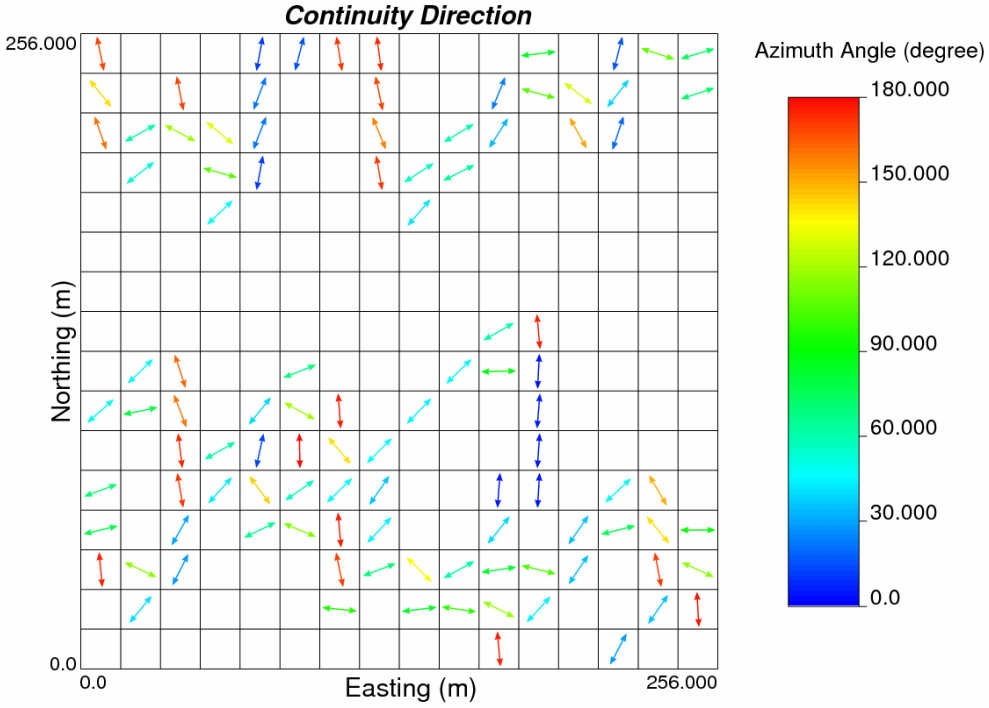

Figure 4.4 The locally varying angles. The arrows show the azimuth angle of continuity direction for each window.

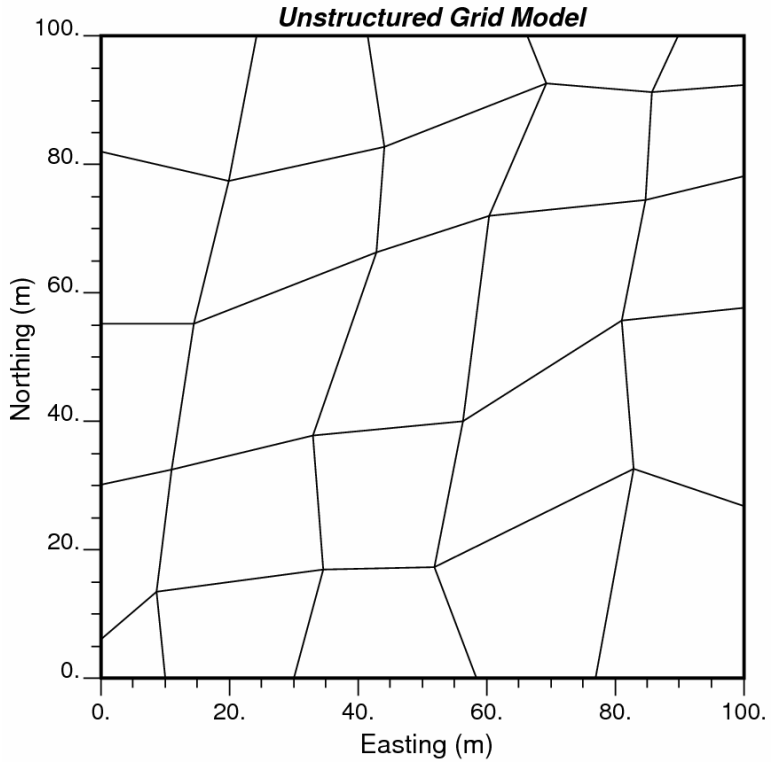

Figure 4.5 The unstructured grid model used for this example.

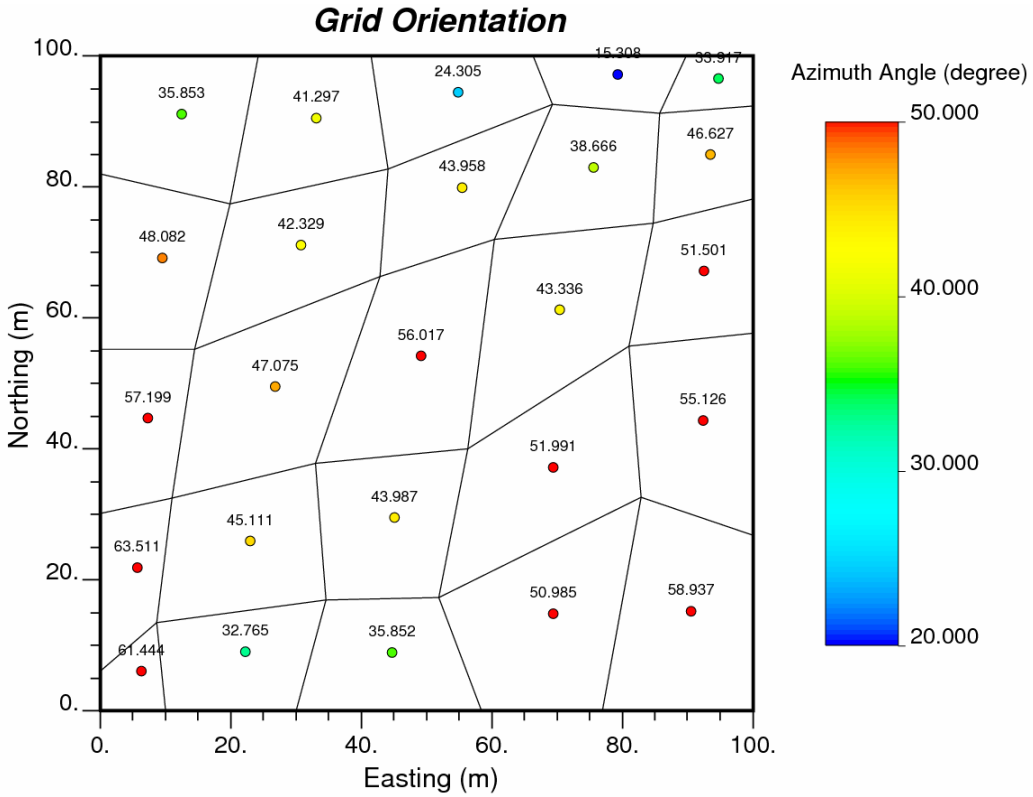

Figure 4.6 The unstructured grid orientation. The points show the centre of mass of each grid and the numbers show the azimuth angle of major direction.

4.3 Discussion

A new method is presented to determine the continuity direction of geological models (continuous and categorical) by analogy to the moment of inertia. The orientation of an unstructured grid block can also be detected with the same approach. Two orthogonal vectors in 2D and three orthogonal vectors in 3D representing the major and minor continuity directions are determined. These angles will be used as a parameters needed for multivariate modelling of permeability tensor.

Chapter 5 Conclusions and Future Work

Unstructured grids are commonly used in reservoir simulation in order to better capture the flow response in complex geological features and or near deviated wells. The characterization of geological heterogeneity within the unstructured block is essential.

Different facies modelling techniques are reviewed and a new approach is examined. The main idea in this method is to simulate each block individually and then add the results to the conditioning data. The method is applied for a synthetic regular and unstructured grid blocks. Each unstructured grid block is locally refined and simulated and then the inside grids are extracted. The connectivity of facies were reproduced well. Since so many conditioning data are used for simulation, the method is computationally expensive. However, the method can be applied for limited number of blocks which are far away from the well data.

Much research has been done in the flow-based upscaling of the permeability. In this thesis a flow-based upscaling technique with random flow boundary conditions is proposed. Different sets of boundary conditions are applied on the coarse block and the flow equation is solved based on the finite difference scheme. For each set of boundary conditions the pressures are randomly assigned to the corner of each grid blocks. Then the results are fed into an optimization technique to fit the components of permeability tensor. The method is flexible to fit full, symmetric and diagonal tensor. The method can be applied for unstructured grid blocks. A Fortran code called *ptensor* is developed to calculate the upscaled permeability for sets of regular or unstructured grid blocks.

Sensitivity analyses on the upscaled permeability tensor show that almost 10 sets of random boundary conditions are sufficient to get a stable permeability tensor.

The size of bounding box significantly changes the error in flow rates. It has been shown that the error decreases to one fourth when the size of bounding box increases three times. However using the larger bounding box is computationally expensive. Further, the permeability values of buffer zone also affect the upscaled permeability tensor. The components of permeability tensor stabilize when the permeability of buffer zone is sufficiently large (for example, $k = 100mD$).

Since the proposed upscaling technique is based on the fine scale permeability, the calculated permeability tensor varying as the fine scale heterogeneity direction is changing. This is confirmed by an example. Fitting the full permeability tensor returns a smaller error in the calculated flow rate compared to the symmetric and diagonal tensor. The error was less than 2% for the specific example considered in this thesis.

A novel approach is developed to automatically determine the continuity direction based on the characteristics of moment of inertia tensor. The method works for both continuous and categorical models. The orientation of an unstructured grid block can also be detected with the same approach. The method is applicable to determine the continuity direction locally when we have a representative training image or available geological model. The result of locally varying angles can be fed into any simulation or estimation techniques which accounts for local variation in continuity direction.

Methodologies presented in Chapter 2 to Chapter 4 can be used to calculate the required parameters for multivariate modelling of permeability tensor on unstructured grid block. The multivariate space of the geological continuity, grid geometry, and permeability characteristics is high dimensional. For example, there may be up to 20 variables describing geological parameters (facies, porosity, directions and magnitude of continuity), up to 20 variables describing each grid element (size and orientation),

up to nine variables describing the permeability tensor. There are other variables including boundary conditions, the spatial distribution of grid blocks etcetera. One could imagine a multivariate distribution with more than 100 dimensions.

Future Work

Based on the methods explained in this thesis, we have the appropriate tools to characterize the permeability tensor for any corner points unstructured grid blocks and to automatically determine the continuity direction of geological setting and unstructured grid cell orientation.

We have seen that the permeability tensor depends on the geological continuity direction and also the unstructured grid orientation. An interesting future research would be to establish a relationship between these three factors.

Another research avenue is to generate the library of multivariate distribution of parameters for unstructured grid blocks. Having a large multivariate distribution library would enable us to populate the permeability tensor for any unstructured grid blocks without using the upscaling techniques. Data points to inform this multivariate distribution could be created by processing high resolution training images through flow simulation. The high dimensional distribution could be modeled with a variety of techniques.

Bibliography

Aasum, Y., Kasap, E. and Kelkar, M., 1993, Analytical Upscaling of Small-Scale Permeability Using a Full Tensor, *SPE paper 25913*, 14 p.

Ababou, R., 1988, Three-dimensional Flow in Random Porous Media, Ph.D. dissertation, Massachusetts Institute of Technology, Cambridge, MA, USA.

Aziz, K, 1993, Reservoir Simulation Grids: Opportunities and Problems, *Journal of Petroleum Technology (JPT)*, Society of Petroleum Engineers, p.658-663.

Bear, J., 1972, Dynamics of Fluids in Porous Media, American Elsevier Pub. Co., New York, 764 p.

Beer, Ferdinand P. and E.Russell Johnston, Jr., 1988, Vector mechanics for Engineers: *Statistics and Dynamics* (5^{th} ed). McGraw-Hill, 1280 p.

Cardwell, W.T. and Parsons, R.L., 1945. Averaging permeability of heterogeneous oil sands. *Trans. Am.Inst. Min. Metall. Pet. Eng.*, 160: 34-42.

Caers, J. 2005, *Petroleum Geostatistics*, Society of Petroleum Engineers, TX, USA, 88 p.

Castellini, A., 2001, *Flow Based Grids for Reservoir Simulation*, M.Sc. Thesis, Stanford University, CA, USA, 79 p.

Desbarats, A.J. and Dimitrakopoulos, R., 1990. Geostatistical modeling of transmissivity for two dimensional reservoir studies. *SPE Formation Evaluation*, December.: 437-443.

Deutsch, C.V., 1987, *A Probabilistic Approach to Estimate Effective Absolute Permeability*, M.Sc. Thesis, Stanford University, CA, 165 p.

Deutsch, C.V., 1989. Calculating effective absolute permeability in sandstone/shale sequences. *SPE Formation Evaluation*, September: 343-348.

Deutsch, C.V., 1992, *Annealing Techniques Applied to Reservoir Modeling and the Integration of Geological and Engineering (Well Test) Data*, PhD thesis, Stanford University, CA, 296 p.

Deutsch, C.V. and Wang, L., 1996, Hierarchical Object-based Stochastic Modeling of Fluvial Reservoirs, *Mathematical Geology*, 28(7):857-880.

Deutsch, C.V. and Journel, A.G. 1998. *GSLIB: Geostatistical Software Library: and User's Guide, 2nd Ed*., New York: Oxford University Press, 369 p.

Deutsch, C.V., 1998. "Cleaning Categorical Variable (Lithofacies) Realization with Maximum A-Posteriori Selection", *Computer & Geosciences*, Vol. 24, No. 6, p.551-562.

Deutsch, C.V., Tran, T.T. and Xie., Y.L., 2001, A preliminary Report on: An Approach to Ensure Histogram Reproduction in Direct Sequential Simulation, *Center for Computational Geostatistics*, University of Alberta, Report: 3.

Deutsch, C. V., 2002. Geostatistical Reservoir Modeling. New York, Oxford University Press, 376 p.

Durlofsky, L.J., 1991, Numerical Calculation of Equivalent Grid Block Permeability Tensors for Heterogeneous Porous Media, *Water Resources Research*, 27: 699-708.

Edwards, G. M., 1998, Simulation with a Full Tensor Coefficient Velocity Field Recovered from a Diagonal Tensor solution, *SPE paper 4907*, p. 383-391.

Galli A., Beucher H., Le Loc'h G., Doligez B., and Heresim Group, 1994, The pros and cons of the truncated gaussian method. In M. Armstrong and P.A. Dowd (eds), *Geostatistical Simulations*, Dordrecht : Kluwer, pp 217-233.

Gelhar, L.W., and Axness, C.L., 1983, Three-dimensional Stochastic Analysis of Macrodispersion in Aquifers, Water resources Research, 19, 161-180.

Georgsen, F. and Omre, H., 1993, Combining Fibre Process and Gaussian Random Functions for Modeling Fluvial Reservoirs, In A. Soares, editor, *Geostatistics Troia*, volume 2, p. 425-440, Kluwer.

Gomez-Hernandez, J.J. and Wen, X.H., 1994, Probabilistic assessment of travel times in groundwater modeling, *Journal of Stochastic Hydrology and Hydraulics*, 8(l): 19-55.

Gomez-Hernandez, J.J. and Journel, A. G., 1994, Stochastic characterization of grid block permeability, *SPE Formation Evaluation*, 9:93-99.

Guardiano, F. and Srivastava, M., 1993, Multivariate geostatistics, Beyond bivariate moments, *in* Soares, A. ed., *Geostatistics Tro*ia '92. v. 1, p. 133-144.

Hatloy, A.S., 1995, Numerical Facies Modeling Combining Deterministic and Stochastic Method, In J.M. Yarus and R.L. Chambers, editors, *Stochastic*

Modeling and Geostatistics: Principles, Methods and Case Studies, p. 109-120, AAPG Computer Applications in geology, No. 3.

Holden, L. and Lia, O., 1992, A Tensor Estimator for the Homogenization of Absolute Permeability, *Transport in Porous Media*, 8:37-46.

He, C., 2000. *Upscaling to general quadrilateral grids*. M.Sc. thesis, Stanford University, Stanford, CA, 36 p.

He, C., 2004. *Structured flow-based Gridding and Upscaling for Reservoir Simulation*. PhD. thesis, Stanford University, Stanford, CA, 191 p.

Journel, A.G. and Alabert, F.G., 1989, Non-Gaussian Data Expansion in the Earth Sciences, *Terra Nova*, 1:123-134.

Journel, A.G. 1983, Nonparametric Estimation of Spatial Distributions, *Mathematical Geology*, Vol. 15, No. 3, p.445-468.

Kelkar, M. and Perez, G., 2002, *Applied Geostatistics for Reservoir Characterization*, Society of Petroleum Engineers Inc., Richardson, TX, 264 pp.

King, P.R., 1989, The use of renormalization for calculating effective permeability, *Transport in Porous Media*, 4(l): 37-58.

King, M.J., 1993, Application and Analysis of Tensor Permeability to Crossbedded Reservoirs, *SPE paper 26118*, Western Regional Meeting, Anchorage, Alaska, USA.

Le Loc'h G., Galli A., 1997, Truncated plurigaussian method: theoretical and practical points of view. In E.Y. Baafi and N.A. Schofield (eds), *Geostatistics Wollongong '96*, Dordrecht : Kluwer, vol. 1, pp. 211-222.

Leuangthong, O., Prins, Deutsch, C.V., 2006, SGSIM_LVA: Gaussian Simulation with Locally varying Angles, In *Centre for Computational Geostatistics* Report Eight, University of Alberta.

Manchuk, J., Leuangthong, O., and Deutsch, C.V. 2004, Direct Geostatistical Simulation on Unstructured Grids, in O. Leuangthong and C. Deutsch, eds., *Geostatistics Banff 2004*, vol. 1, Springer Science+Business Media, p. 85-94.

McLennan, J. A., 2002, The effect of the simulation path in sequential gaussian simulation, In *Centre for Computational Geostatistics* Report Four, Edmonton, Alberta, University of Alberta.

Omre, H., 1992, Heterogeneity Models, In *SPOR Monograph: Recent Advances in Improved Oil Recovery Methods for North Sea Sandstone Reservoirs*, Norway, Norwegian Petroleum Directorate.

Palagi, C. L. and Aziz, K. (1991). Use of Voronoi grids in reservoir simulation, *SPE paper 22889* presented at the *SPE* Annual Technical Conference and Exhibition, Dallas, Texas, 6-9 October.

Prevost, M., 2003. *Accurate Coarse Reservoir Modeling Using Unstructured Grids, Flow-based Upscaling and Streamline Simulation*. PhD thesis. Stanford University, Stanford, CA, p.222.

Reference Manual of Eclipse Simulator, Geoquest Simulation Software Manuals, *Schlumberger*, 2005A.

Seifert, D. and Jensen, J.L. 1999, Using Sequential Indicator Simulation as a Tool in Reservoir Description: Issues and Uncertainties, *Mathematical Geology*, Vol. 31, No. 5, p. 527-550.

Strebelle, S.,2002, Condiotional Simulation of Complex Geological Structures Using Multiple-point Statistics, *Mathematical Geology*, 32(9):2937-2954.

Tran, T.T., 1995. *Stochastic Simulation of Permeability Field and their Scale up for Flow Modeling*, Ph.D. thesis, Stanford University, CA, p.237.

Verma, S. and Aziz, K., 1997, A Control Volume Scheme for Flexible Grids in Reservoir Simulation, *SPE paper 37999* presented at the *SPE Reservoir Simulation Symposium, Dallas*, TX, June 8-11.

Warren, J.E. and Price, H.H., 1961, Flow in heterogeneous porous media, *Society of Petroleum Engineering Journal*, 1: 153-169.

Wen, X.H., Durlofsky L.J., and Edwards, M.G., 2003, Upscaling of Channel Systems in Two Dimensions Using Flow-Based Grids, *Transport in Porous Media*, 51: 343-366.

White, C.D. and Horne, R.N., 1987, Computing absolute transmissivity in the presence of fine-scale heterogeneity, *SPE paper 16011*, pp. 209-221.

Appendix A

Fortran Code: Permeability Tensor

(*ptensor*)

The GSLIB-style program, called *ptensor*, is developed to calculate the permeability tensor for 2-D and 3-D unstructured grid block. It is based on the finite difference solution of single-phase, steady-state flow equation and optimization method. The *ptensor* program permits different options related to the shape of coarse grid (Polygon in 2-D or corner point geometry in 3-D), size of the buffer zone, the permeability value inside this zone, and an option to fit full, symmetric or diagonal tensor. The parameters required for this program are:

```
                          Parameters for PTENSOR
                         ************************
Line START OF PARAMETERS:
  1  2                    -2-D (X/Y) or 3-D (X/Y/Z)
  2  perm.dat             -input data faile with permeability
  3  1 2 3 0 0 0          -columns for kx,ky,kz,ky/kx,kz/kx
  4  50  50  10           - input : nx, ny, nz
  5  1.0 1.0 1.0          - input : dx, dy, dz
  6  ptensor.out          -file for permeability tensor output
  7  ptensor.dbg          -file for debugging output
  8  usg.dat              -file for unstructured grid
  9  1                    - Number of grids
 10  1 1 1 1 1 1          -Buffer zone size:X-left,X-right,Y-left,Y-right,Z-left,Z-
                          right
 11  1                    -Buffer zone : Homogeneous(1), Heterogeneous(0)
 12  20                   - if (1),constant permibility value
 13  20                   -Number of Boundary Conditions
 14  69069                -random number seed
 15  1                    -fitting option: 1=diag, 2=symm, 3=full
 16  0.001  5000          -minimum objective function, max per
```

In the first line there is an option to choose the dimension. Both 2-D and 3-D cases are acceptable. The information about the fine scale permeability data file are input in Lines **2** and **3**. The number and size of grid cells in the input file should be specified in Lines **4** and **5**. In Line **6** and **7,** the name of output and debugging files are specified. The debugging file comprised of the flow simulation results for each coarse

grid. The file for unstructured grids is specified in line **8**. In unstructured grid file the number of corner points for each grid is provided first. In the following lines, the coordinates are specified by two triples of X, Y and Z coordinates, representing two corresponding points in upper and lower planes (description of 3-D grids are described in the paper). Below is an example of acceptable unstructured grid file.

```
Unstructured grid file
4
 53.2     48.6    7        53.2     48.6     3
 38.2     30      7        38.2     30       3
 57.4     12.9    7        57.4     12.9     3
 87.5     40.5    7        87.5     40.5     3
5
 8        10      7        8        10       3
 20       10      7        20       10       3
 29       6       7        29       6        3
 25       5       7        25       5        3
 10       5       7        10       5        3
```

Six integer numbers in line **10** control the size of buffer. Each integer value shows the number of fine grid which should be added to the smallest rectangular region. For example “2 2 2 2 2 2” means that the bounding box should be expanded by two fine grids at each side. There is an option for the permeability value of buffer zone. Lines **11** and **12** enable the user to choose if the buffer zone is homogeneous or heterogeneous and what is the homogenous permeability value is (if put 1 in line 11). In the line **13**, the number of random boundary conditions for which the flow simulation should be solved is specified. The random number seed is specified in line **14**. It should be a large odd number. Three options are available to fit the tensor (full, symmetric or diagonal). Line **15** corresponds to these options. The minimum objective function (error) and the number of iterations for tensor fitting are specified at the last line.